Small-Scale Variability in Saturn's Lower Ionosphere

March 16, 2012

Katia I. Matcheva[1]

Daniel J. Barrow[1,2]

1 Department of Physics, University of Florida, Gainesville FL 32611-8440

katia@phys.ufl.edu

2 Buchholz High School, Gainesville FL 32606

barrowdj@gm.sbac.edu

Corresponding Author:

Katia I. Matcheva

Department of Physics, University of Florida, P.O. Box 118440, Gainesville FL 32611-8440

e-mail: katia@phys.ufl.edu

phone: (352) 392 0286

Abstract

We perform and present a wavelet analysis on all 31 Cassini electron density profiles published to date (Nagy et al., 2006; Kliore et al., 2009). We detect several discrete scales of variability present in the observations. Small-scale variability ($S < 700$ km) is observed in almost all data sets at different latitudes, both at dawn and dusk conditions. The most typical scale of variability is 300 km with scales between 200 km and 450 km being commonly present in the vast majority of the profiles. A low latitude dawn/dusk asymmetry is noted in the prevalent scales with the spectrum peaking sharply at the 300 km scale at dusk conditions and being broader at dawn conditions. Compared to dawn conditions the dusk ionosphere also shows more significant variability at the 100 km scale. The 300 km vertical scale is also present in the few available profiles from the Northern hemisphere. Early observations from 2005 show a dominant scale at 350 km whereas later in 2007-2008 the spectrum shifts to the shorter scales with the most prominent scale being 300 km. The performed wavelet analysis and the obtained results are independent of assumptions about the nature of the layers and do not require a definition for a "background" electron density profile.

In the second part of the paper we present a gravity wave propagation/dissipation model for Saturn's upper atmosphere and compare the wave properties to the characteristics of the observed electron density variability at different scales. The general features observed in the data are consistent with gravity waves being present in the lower ionosphere and causing layering of the ions and the electrons. The wave-driving mechanism provides a simultaneous explanation for several of the properties of the observed variability: (i) Lack of variability in the electron density above the predicted region of wave dissipation; (ii) In most cases the peak amplitude of variability occurs within the altitude range for dissipation of gravity waves or below; (iii) Shorter scales have smaller amplitudes than the longer scales; (iv) Shorter scales are present at lower altitudes whereas longer scales persist to higher altitudes; (v) Several layers often form a system of equally spaced maxima and minima that can be traced over a large altitude range.

Keywords: atmospheres, composition; atmospheres, dynamics; ionospheres; Saturn, atmosphere.

1 Introduction

Our current knowledge of the structure of the ionosphere of Saturn is based mostly on spacecraft radio occultations (Pioneer 10 and 11, Voyager 1 and 2, and Cassini) and observations of the auroral emission in the UV and the near IR. In addition, the detection and monitoring of the Saturn Electrostatic Discharges (SED) by the Voyager Planetary Radio Astronomy (PRA) experiment and by the Cassini Radio and Plasma Wave Science (RPWS) experiment carry information about the maximum electron density and its evolution with time (Warwick et al., 1981; Warwick et al., 1982; Fischer et al., 2006; Fisher et al., 2011). The thermal structure of the atmosphere at ionospheric heights is constrained by stellar and solar occultations performed by the Voyager UVS and the Cassini UVIS teams (Festou and Atreya, 1982; Smith et al., 1983; Nagy et al., 2009). The observations reveal an ionosphere with complex vertical structure which strongly varies with time and latitude (Nagy et al., 2006; Kliore et al., 2009).

Previous theoretical models of Saturn's ionosphere have focused on its overall structure (the maximum of the electron density and total electron content of the ionosphere) and its latitudinal and time dependence in an attempt to capture the main physics and chemical processes that control the ionosphere (Moore et al., 2010). Difficulties arise from the unconstrained abundance of vibrationally excited H_2 molecules and the unknown amount of water influx from Saturn's rings, both of which are bound to have a strong impact on the ionospheric chemistry. Both quantities have been previously used as free parameters to reduce the lifetime of H^+ ions and to decrease the predicted values for the maximum of the electron density in order to fit the observations (McElroy, 1973; Connerney and Waite, 1984; Majeed and McConnell, 1991, 1996; Moses and Bass, 2000; Moore et al., 2004). Furthermore, very little is known about the dynamics of Saturn's ionosphere since the observations contain no direct information about the wind system at these altitudes.

The Cassini radio observations, resulting in 31 published electron density profiles to date, provide us with the most detailed picture so far of the structure of Saturn's ionosphere. The observations have been made during the first phase of the Cassini mission from 2005 to 2008, corresponding to southern hemisphere summer and early fall. The following features have

been previously pointed out in the literature: 1) The maximum electron density as well as the total electron content (TEC) increase with latitude with a maximum in the polar regions (Moore et al., 2010). 2) At low latitudes the dawn electron density peak is smaller and occurs at higher altitudes (referred to as dawn/dusk asymmetry) (Nagy et al., 2006; Kliore et al., 2009). 3) A complex system of sharp layers of enhanced electron density is observed in the lower ionosphere at most latitudes. 4) Some profiles exhibit large vertical regions of near depletion of electrons (referred to as bite-outs).

In this paper we investigate the small-scale vertical layering present in a significant fraction of the 31 Cassini electron density profiles of Saturn published in the literature to date. Multiple layers in the electron density are observed in virtually all Cassini profiles as well as in the Voyager and Pioneer profiles although some of them do not extend to very low altitudes. The layers are seen in dusk and dawn conditions at low, mid and high latitudes. The number of identifiable layers, the magnitude of the electron density peaks, the vertical scale (thickness) of the layers, and the spacing between the individual peaks vary. In this paper we present a statistical analysis for the scale and the magnitude of the vertical variations present in the individual Cassini electron density profiles. The large number of observations allow us to study the spectrum of the vertical variability at different latitudes and to even compare dawn and dusk conditions.

It is well known that the terrestrial night-time ionosphere often displays similar systems of narrow layers of electrons which are usually attributed to atmospheric waves or plasma instabilities (Kelley, 1989). Similar layers have also been observed in the Galileo J0-ingress electron density profile of Jupiter which samples the ionosphere at dusk conditions (Hinson et al., 1997). This system of layers has been successfully modeled as a signature of an atmospheric gravity wave propagating in Jupiter's thermosphere (Matcheva et al., 2001; Barrow and Matcheva, 2011). The corresponding dawn electron density profile of Jupiter however showed very different ionospheric structure with no well pronounced small-scale layers.

In the second part of this paper we model the propagation of atmospheric gravity waves in Saturn's thermospheric/ionospheric region and compare the predicted properties of the waves to the spectral characteristics of the observed variability in the electron density.

2 Vertical variability in the electron density

The first step in our analysis is to study the variability in the data with minimum theoretical assumptions about the nature of the fluctuations and/or the state of the ionosphere. We perform a wavelet analysis on all 31 electron density profiles published to date by the Cassini Radio Science Team to identify the prevalent scales of variability in the vertical electron density distribution. A brief mathematical introduction to the theory and application of the wavelet analysis can be found in Torrence and Compo (1998) along with a downloadable software for public use. For the purpose of our study we use the continuous wavelet transform together with the Morlet wavelet basis as it provides us with optimal scale discrimination and vertical resolution. For a discrete series of measurements, x_n, $(n = 0...N-1)$, with equal spacing δt (in our case the sampling is done in space rather than in time) the functional form of the Morlet wavelet is

$$\psi_0(\eta) = \pi^{-1/4} e^{i\omega_0\eta} e^{-\eta^2/2}, \tag{1}$$

where $\eta = \frac{n\delta t}{S}$ is a dimensionless "time" parameter, ω_0 is the dimensionless frequency, and S is a scale of variability (analogous to the wavelength in a Fourier transform). In this study $\omega_0 = 6$.

The wavelet coefficients $W_n(S)$ for a given scale s and position n are then calculated using the continuous wavelet transform

$$W_n(S) = \sum_{n'=0}^{N-1} x_{n'} \psi_0^* \left[\frac{(n'-n)\delta t}{S} \right], \tag{2}$$

where $(^*)$ indicates a complex conjugate. Similar to the Fourier coefficients the square of the wavelet coefficients presents the energy within a given scale of variability. In many cases the wavelet analysis is a preferred tool for data analysis as it also shows how the magnitude of these variations changes within the length of the data set. In our analysis the calculated wavelet coefficients (2) are normalized so that he square of the wavelet coefficient is equal to the square of the amplitude of the observed variation rather than the power of the present scales.

Figure 1

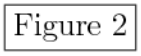

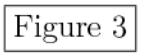

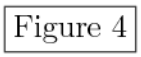

The results from the wavelet analysis for selected latitudes are shown in Figs. 1-4. The results for the remaining 27 cases are shown in the Appendix in Figs. A.1-A.27. Figure 1 shows the analysis of a high latitude observation (72°S at dusk), Fig. 2 presents a mid latitude case (28°S at dusk), Figs. 3 and 4 correspond to low latitude conditions at dusk (3°S) and dawn (9°S), respectively. The choice of latitudes is to illustrate the fact that layering in the ionosphere of Saturn is present at all latitudes at diverse local conditions and time of the day.

Each of the figures has three panels showing the local electron density profile (left panel), a color map of the variations $Re(W_n(S))$ present in the data at different scales as a function of altitude (central panel), and a color map of the amplitude of the variations $|W_n(S)|$ at different scales as it changes with height (right panel). The variations N_e' are normalized to the peak electron density, $N_{e,max}$, and the result $\frac{N_e'}{N_{e,max}}$ is presented in percentage. By definition the variation cannot exceed 50% . The contours are drawn at 5% intervals. A vertical slice through the amplitude color map shows how the amplitude at a given scale S changes with height. A horizontal cut through the map at a given altitude produces the spectrum of the scales present at this height. Similar to the Fourier analysis the wavelet analysis suffers from edge effects. The effect is scale dependent and results in distortion of the power at the edge of the map at a distance one scale length away from the edge.

At this point the wavelet analysis is performed without any assumption about the nature of the layers and the origin of the vertical variability. There is no predefined "background" ionospheric state. This is reflected in the presence of significant power at very large scales ($S > 800$ km) which are likely to represent the overall structure of the ionosphere resulting form ion chemistry and diffusion. The wavelet analysis provides information about the dominant scales of variability in the data, the amplitude of the fluctuations and how this amplitude varies with height. The last point makes the wavelet analysis particularly valuable in studying altitude dependent periodic phenomena. A summary of the wavelet results

(detected scales S, maximum amplitude $\Delta N_{e,max}$, peak altitude Z_{max}) presented in Figs. 1 through 4 is shown in Table I.

Table I

As each electron density profile is different and every one of them provides a clue about the nature of the variability we present the wavelet analysis of all remaining 27 electron density profiles in the Appendix for the benefit of the reader. Based on the wavelet analysis of all 31 occultations we can make the following observations: (i) Multiple layers are present at all latitudes both at dusk and dawn conditions. (ii) Large amplitude variability and layering is more common in the lower ionosphere (below and at the main electron density peak) though small amplitude variation in the electron density is sometimes present throughout the entire observed altitude range (see for example occultation S11 exit, Fig. A.6) . (iii) A number of profiles exhibit 2-3 dramatic sharp layers (S68 entry, Fig. 2) while other profiles have embedded small-amplitude electron density variations which one can trace in the data for several cycles over a long distance (S07 exit, Fig. 4). (iv) In a few cases the layers of electrons are separated by regions that are completely depleted of electrons (S47 exit, Fig. A.15).

Figure 5

Figure 6

To illustrate the full diversity of scales detected in the Cassini electron density profiles we present a statistical summary of the results from the wavelet analysis of all 31 profiles. Figure 5 shows the fraction of profiles in which a scale S is detected with an amplitude larger than 5%. The scales are grouped in bins of $\Delta S = 50$ km and range from $S = 50$ km to $S = 1000$ km. Note that the smallest scale used in the wavelet analysis is 16 km; however, no significant power is detected at scales smaller than 50 km. To search for latitudinal trends we present similar histograms after sorting the observations into "high latitude", "mid latitude" and "low latitude". One can also compare dawn and dusk conditions. The results are shown in Fig. 6, where we consider low latitude profiles only. The counts are normalized by the total number of available profiles: 8 for dusk and 8 for dawn conditions. In contrast to a power

spectrum the presented histograms do not contain information about the magnitude of the variations. They simply reflect the frequency of occurrence of a given scale of variability with an amplitude in excess of 5%. Based on the histograms on can make the following conclusions:

1) Overall the most typical scale of vertical variability is 300 km. Only three out of the 31 profiles show no fluctuations at scales less than 450 km. The scale values are approximate as the width of the bins is 50 km.

2) The midlatitudes are dominated by 300 km variability whereas at low latitudes the 350 km scale prevails. High latitudes show a broad range of scales shorter than 500 km.

3) At low latitudes the dusk ionosphere most often shows the presence of a 300 km scale and the frequency of occurrence of 250 km and 350 km scales is reduced by half in comparison to dawn observations.

4) There is a significant variability at the 100 km scale, however, the amplitude of the fluctuations are typically less than the 5% cutoff and the variability is confined to the very bottom of the observed region. The 100 km scale is most notable at low latitudes at dusk conditions.

Figure 7

The analyzed observations are done over a time period of a few years starting in 2005 through 2008. It is reasonable to expect that the spectrum of the present scales might evolve in time over the years. We compare the observations made in 2005 with the observations made later in the mission (late 2007-2008). The corresponding histograms are shown in Fig. 7. The 2005 observations are done within 4 months and are exclusively at low latitudes. The second group of observations (2007-2008) are from high and middle latitudes and one low latitude. A few observations are made in 2006 or early 2007. Since they are significantly separated in time from the other two groups we do not include them in this analysis. With this time selection the scatter in the histograms in Fig. 7 is decreased and we see a dominant 350 km scale for the 2005 low latitude observations and a dominant 300 km for the 2007-2008 observations. Although the shift towards shorter scales is well pronounced one should keep in mind that the size of the histogram bins is 50 km and the shift is within the uncertainties

of the analysis. It is also possible that the shift reflects the difference in the sampled latitudes rather than a real seasonal change.

Finally most of the observations in our analysis are from the southern hemisphere with only 5 electron density profiles from the northern hemisphere. At this point one cannot make any statistical comparison based on hemispheric separation except to note that the electron density profiles in the northern hemisphere also have sharply peaked layers in the lower ionosphere with the 300-350 km scale present in all five of the profiles (see Appendix Figs. A.4 , A.7, A.12, A.24, and A.26). It would be interesting to extend this statistical analysis to the northern hemisphere as new observations become available.

3 Atmospheric Gravity Waves

The wavelet analysis in Section 2 demonstrates the presence of a wide range of scales of variability in the electron density profiles which give rise to the layered appearance of Saturn's lower ionosphere. The nature of these layers is open for discussion. In this paper we investigate the hypothesis that the observed small-scale layering is caused by atmospheric gravity waves that propagate in Saturn's upper atmosphere.

Atmospheric gravity waves are buoyancy driven oscillations of a parcel of air which in a stable atmosphere can propagate over a large distance. In contrast to sound waves, gravity waves are transverse waves with frequency smaller than the buoyancy frequency of the atmosphere. On the other hand the period of a gravity wave is smaller than the period of a typical Rossby wave so that the planetary rotation does not significantly impact its propagation. The dispersion relation for a hydrostatic gravity wave in a conservative atmosphere is given by:

$$k_z^2 = \frac{k_h^2 N^2}{\omega^2} - \frac{1}{4H^{*2}}, \tag{3}$$

where k_z and k_h are the vertical and the horizontal wave numbers, respectively, N is the buoyancy frequency, H^* is the atmospheric density scale height, and ω is the wave frequency.

Atmospheric gravity waves are easily excited by transient atmospheric phenomena, atmospheric instabilities, weather fronts, convective storms, etc. In a conservative atmosphere with no wind shear the amplitude of the waves grows exponentially with altitude as the

background density decreases with height. As a result small-amplitude waves generated in the lower atmosphere can have large amplitudes by the time they reach the thermosphere and can leave observable signatures in the temperature structure and the wind profile of the atmosphere at these heights. Not all gravity waves make it to very high altitudes (low pressure levels) as they are subject to a number of dissipative processes. Along their path they might get absorbed in the mean zonal wind or reflected by strong temperature gradients. Waves with amplitudes that are big enough to drive the local temperature gradient beyond the dry adiabatic lapse rate become unstable and overturn, depositing energy and momentum in the background atmosphere. In addition, waves that reach low pressure levels are dissipated by diffusive processes like molecular viscosity and heat conduction. For a detailed mathematical treatment of wave propagation and dissipation we refer the reader to Hines (1974), Lindzen (1981), and Walterscheid (1981).

In our work we use an atmospheric gravity wave model that is based on the assumptions that the waves are linear and hydrostatic, that the atmospheric temperature is slowly varying with height and that the vertical gradient of the mean zonal wind is zero. The model includes wave dissipation due to molecular viscosity, eddy diffusion, and thermal conduction. We keep the amplitude of the waves below the breaking point at all heights. The model has been originally developed for Jupiter and subsequently adapted for Saturn. The mathematical details and the numerical implementation of the model are presented in Matcheva and Strobel (1999) and Matcheva et al. (2001) and summarized below. A single linear wave is imposed at the bottom of the simulated region by defining the wave vertical and horizontal wavenumbers (k_{z0} and k_h, respectively), vertical velocity amplitude $\Delta W(z_0)$ and phase. We then solve the dispersion equation Eq. (4) for the complex and real parts of the vertical wavenumber ($k_z = k_{zr} + ik_{zi}$), and the resulting velocity fields as the wave propagates up in the atmosphere (Eqs. (5) and (6)).

$$k_z^2 = \frac{k_h^2 N^2}{\tilde{\omega}(\tilde{\omega} + i\beta)} - \frac{1}{4H^{*2}}\left[1 - 2\frac{dH^*}{dz}\right] \tag{4}$$

$$\Delta W(z) = \Delta W(z_0)\left(\frac{k_{zr0}}{k_{zr}}\right)^{1/2} exp\left[\int_{z_0}^{z}\left(\frac{1}{2H^*} - k_{zi}\right)dz\right] \tag{5}$$

$$\Delta V(z) = \Delta W(z)\left(\frac{k_{zr}}{k_h}\right)\sqrt{1 + \left(\frac{k_{zi}}{k_{zr}} + \frac{1}{H^* k_{zr}}\right)^2} \tag{6}$$

In Eq. (4) $\tilde{\omega}$ is a complex frequency with a real part corresponding to the wave's actual frequency and a complex part resulting from the viscous dissipation, β is a dissipation factor showing the effect of thermal conductivity. The analytical definitions for $\tilde{\omega}$ and β are given in Matcheva et al. (2001). The bottom boundary of the model is at 500 km and the top boundary is placed at 2500 km above 1 bar pressure level. The vertical step of the calculations is 1 km.

4 Structure of the neutral atmosphere

The background neutral atmosphere used for the wave model is summarized in Fig. 8. Similar to Jupiter the dominant neutral species in Saturn's atmosphere are H_2, He, and CH_4 with atomic hydrogen becoming important at high altitudes. Below the methane homopause (around 900 km above the 1 bar pressure level) eddy diffusion dominates and the atmosphere is well-mixed. The eddy diffusion coefficient incorporated in the model varies with height and is taken from Moses et al. (2000). Above the homopause, where molecular diffusion is dominant, the species separate diffusively according to their individual scale heights and the CH_4 and He mixing ratios decrease quickly with altitude. H_2 is dominant up to roughly 3000 km at which point H becomes the main neutral component. The neutral densities are calculated using the mixing ratios for He and CH_4 at the bottom boundary of the model and are taken from Conrath and Gautier (2000). The resulting neutral density profiles are in good agreement with the composition model from Moses and Bass (2000).

Figure 8

The choice of temperature profile is essential for modeling atmospheric gravity waves as the wave propagation is impacted by the thermal structure through the buoyancy frequency (see Eq. 3). In addition, the environmental lapse rate controls the maximum amplitude for a given vertical wavelength before the wave becomes unstable and overturns.

The thermal structure of Saturn's troposphere and lower stratosphere is well constrained by Cassini CIRS observations (Fletcher et al., 2010). Middle stratospheric regions are accessible by ground based stellar occulations (Hubbard et al., 1997; Harrington et al., 2010)

whereas the upper stratosphere and lower thermosphere have been sampled by the Voyager and Cassini stellar and solar occultations (Festou and Atreya, 1982; Smith et al., 1983; Lindal 1992). The CIRS temperature maps of the lower stratosphere show the temperature at the 1 mbar level to vary by more than 30 K from pole to pole. The number of temperature profiles in the upper stratosphere and thermosphere are limited, they have significant uncertainties (about 100 K), and show large variability (Nagy et al., 2009). Temperature estimates at the top of the thermosphere vary from 300 K to 500 K (Nagy et al., 2009). In view of these uncertainties we use a generic temperature profile shown in Fig. 8 which captures the main observed features: a relatively isothermal stratosphere at $T = 137$ K at the bottom of the modeled region, followed by a fast temperature increase between 800 km and 1300 km and topped by an isothermal layer at $T = 417$ K. This temperature profile closely follows the T profile compiled by Moses et al. (2000). Subsequently we keep in mind that the temperature in the thermosphere is likely to vary from latitude to latitude as well as with time.

5 Propagation and dissipation of atmospheric gravity waves

In this section we address the question if and what type of gravity waves can reach the altitude region of interest (500-2500 km above 1 bar level) and what are the observational constraints on the wave parameters. As we discuss in Sec. 3, not all gravity waves can reach the upper atmosphere. They can be absorbed, reflected or dissipated as they travel through the lower atmosphere. Undoubtedly the wind system in the stratosphere has a strong filtering effect on the tropospheric waves which can reach the ionosphere. At this point, however, we do not know the origin of the waves, nor the wind system in the upper stratosphere. Instead we focus on the ability of the waves to overcome dissipative processes like eddy and molecular viscosity and thermal conduction that dominate wave dynamics at high altitudes. These dissipative processes are selective as waves with longer vertical wavelengths and shorter periods tend to be less impacted by the molecular dissipation and can propagate higher in the atmosphere.

Figure 9

Figure 9 illustrates the behavior of the amplitude (vertical velocity, horizontal velocity, and temperature) of three atmospheric gravity waves together with a profile of the vertical wavelength as the waves pass through the modeled region. The three waves have a period of 30 min and vertical wavelength at the bottom of 50 km, 100 km, and 200 km respectively. In agreement with Eq. (5), the vertical velocity amplitude peaks at an altitude where dissipation overcomes the natural exponential growth of the wave:

$$k_{zi} = \frac{1}{2H^*}. \tag{7}$$

We refer to this altitude as the altitude of wave dissipation (z_d), though the dissipation occurs in a rather broad altitude range and not just at this particular location. Above this altitude the magnitude of the observable signature of the wave is decreasing as the the amplitude becomes smaller. The wave with the longest vertical wavelength has the highest dissipation altitude as the periods of the waves are the same. In contrast to the vertical velocity the amplitude of the horizontal velocity of the 100 and the 200 km waves has two peaks (Fig. 9b,c). The top one marks the region where the dissipation becomes dominant whereas the bottom peak results from the variation of the background temperature and the subsequent changes in the atmospheric stability. The bottom peak or hump is at the same altitude for waves of all scales ($z = 1100$ km) whereas the location of the top peak is scale-dependent. A variable vertical wavelength together with a double-peaked amplitude profile can be an indication for a strong temperature gradient in the background atmosphere. However, this is not a unique interpretation as varying background winds can have a similar effect on the wave propagation. Figure 9 also shows the variation of the vertical wavelength with height. The vertical wavelength changes as a result of two separate effects: the variable temperature in the 900-1200 km region and the viscous dissipation itself as it causes the wave fronts to become increasingly more vertical leading to larger vertical wavelengths.

Figure 10

Figure 10 shows the altitude of wave dissipation z_d for a range of vertical wavelengths and periods. We consider vertical wavelengths less than 700 km to comply with the WKB approximation of our gravity wave model and periods between the buoyancy period ($\tau =$

$2\pi/N$) and one Saturnian day ($\sim$ 10 h). Waves with large vertical wavelengths and short periods (larger frequency) dissipate high in the atmosphere. Waves with vertical wavelength shorter than 100 km reach a maximum amplitude at altitudes below 1200 km even for the highest frequencies. This implies that gravity waves can not cause significant electron density layering with a characteristic vertical scale less than 100 km at an altitude above 1300 km. Similarly one can state that waves with vertical wavelength of 300 km reach a maximum amplitude at or below 1600 km. Above 1900 km gravity waves should not cause strong observable signatures with a characteristic scale of 300 km.

Figure 9 also shows that at large periods the dissipation height z_d is only weakly dependent on the wave period, or in other words for a given vertical wavelength waves with a period between 0.5 and 1 Saturn day peak at roughly the same altitude.

The dissipation curves for gravity waves with a period of 30 min and 10 h are plotted on the wavelet coefficient maps for all 31 electron density profiles presented in Figs. 1-4 and in the remaining figures in the Appendix as light solid lines A and B, respectively. The curves can be used as a guide for the range of altitudes where gravity wave signatures can be expected. Roughly one wavelength above line A gravity waves are not expected to cause strong variability in the electron density profile. The best gravity wave candidates would have a signature in the electron density that is maximum in the region between curves A and B. A local maximum in the wavelet map below curve B is still consistent with a gravity wave interpretation. The peak can be caused by background temperature variation and/or local ion chemistry which can modify the response of the ionosphere to the forcing neutral wave. In this case the dissipation altitude of the wave z_d does not coincide with the maximum of the electron density variability.

6 Discussion

In Sec. 2 we analyze the variability of the electron density profiles for characteristic vertical scales and in Sec. 5 we describe the propagation/dissipation of gravity waves in the upper atmosphere. Here we will discuss how compatible the observed variations in the electron density profiles are with gravity wave signatures. We focus on vertical scales shorter

than 700 km with amplitudes larger than 5% in the wavelet maps presented in the Appendix and in Figs. 1-4. While discussing the observed features one should keep in mind that the wave model that we use relies on a generic temperature profile which is kept constant for all latitudes and atmospheric conditions (dawn/dusk for example). Almost certainly the temperature behavior varies from location to location and in time and therefore the exact wave propagation would also vary. Nevertheless we can make the following observations:

• *There is no strong variability (amplitude* $> 5\%$*) at any scale shorter than 700 km above line A.* Noted exceptions are the equatorial observations S11 exit, S12 exit, S13 exit, S44 entry, and the only north high latitude profile S46 exit.

This is consistent with a gravity wave driving mechanism. Line A shown in the wavelet amplitude maps provided in the Appendix indicates the altitude at which a 30 min wave peaks for different vertical wavelengths. The 30 min time scale corresponds to the buoyancy frequency at high altitudes (>1300 km). This is the shortest gravity wave period to be expected at this altitude. The buoyancy period at the homopause is about 15 min.

• *In general, smaller scales of variability are present at lower altitudes whereas larger scales persist to higher altitudes.*

This is also consistent with a gravity wave driving mechanism. As discussed in Sec. 5 waves with short vertical wavelengths dissipate at lower altitudes whereas waves with large vertical wavelengths reach high altitudes before they become impacted by dissipation. The wavelet amplitude maps clearly show a trend of larger scales being present at higher altitudes.

• *In many cases there are several layers with the same vertical scale resembling a wave-train at a fixed wavelength.*

This is consistent with a gravity wave driving mechanism. Although forming layers of enhanced electron density is not restricted to the gravity wave mechanism only, what is specific for the proposed mechanism is the equal spacing between the individual layers (a relatively constant vertical wavelength) and the multiplicity of the layers (the wave can be traced over several wavelengths as the wave train propagates). This is especially true for the smaller-scale , small-amplitude variability detected in the data (see for example S07 exit and S56 exit).

• *Smaller scales have smaller amplitudes whereas larger scales reach much larger ampli-*

tudes.

This is consistent with a gravity wave driving mechanism. The gravity wave amplitude growth is limited both by dissipation and by atmospheric instabilities. The linear wave theory predicts that gravity waves become unstable and overturn when the local temperature gradient exceeds the dry adiabatic lapse rate. Waves with shorter vertical wavelengths are associated with larger vertical gradients and are therefore prone to instabilities at small amplitudes. As a result waves with large vertical wavelengths are allowed to grow to larger amplitudes as they propagate up in the atmosphere.

• *In most cases the peak amplitude occurs within the altitude range for a typical gravity wave dissipation (between lines A and B) or below.*

This is consistent with a gravity wave driving mechanism. The region bracketed between lines A and B in the wavelet maps corresponds to the dissipation altitude for waves with periods between 30 min and 10 hours. In general one can use the location of the observed wave amplitude peak to constrain the wave frequency and horizontal wavelength for a given vertical wavelength using Eq. (3) and (7). However, the observed parameter in the Cassini radio occultations is the variability in the electron density rather than in the temperature or in the wind of the neutral atmosphere. The response of the ionosphere to gravity wave forcing is indeed proportional to the neutral wave amplitude but this is not the only factor that shapes up the amplitude of the induced electron density variations. The magnitude of the effect is limited by local chemistry and modified by the electron density gradient in the background ionosphere (Matcheva et al., 2001; Barrow and Matcheva, 2011; Barrow et al., 2012). The bottom line is that without a careful modeling of the wave-ion interaction and local ion chemistry one cannot predict the location of the peak electron density variability in response to a given wave forcing. Such models exist for Jupiter (Matcheva et al., 2001; Barrow and Matcheva, 2011) and are under development for Saturn (Matcheva and Barrow, in preparation). This prediction is particularly difficult for large-amplitude variations where the variability is of the order of the average electron density and linear perturbation models are inadequate to describe the interaction between the ions and the propagating gravity wave.

7 Conclusions

We perform a wavelet analysis on all Cassini electron density profiles published to date (Nagy et al., 2006; Kliore et al., 2009). The results are shown in the Appendix. We detect several discrete scales of variability present in the observations. Small-scale variability ($S <$ 700 km) is observed in almost all data sets at different latitudes and dawn/dusk conditions. The most typical scale is 300 km but scales between 200 km and 450 km are commonly present in the vast majority of the profiles. A dawn/dusk asymmetry is noted in the prevalent scales with the most often observed scale being 200 km at dawn and 300 km at dusk. Compared to dawn conditions the dusk ionosphere also shows more significant variability in the 100 km scale. The 300 km vertical scale is also present in the few available profiles from the Northern mid and high latitudes. The performed wavelet analysis is independent of assumptions about the nature of the layers and does not require a definition for the "background" electron density profile and thus the results can be used independently of our wave interpretation of the origin of the variability.

In the second part of the paper we present a gravity wave propagation/dissipation model for Saturn's upper atmosphere and compare the wave properties to the characteristics of the observed electron density variability at different scales. The general features observed in the data are consistent with gravity waves being present in the lower ionosphere and causing layering of the ions and the electrons. Though this is not a unique interpretation, the wave-driving mechanism provides simultaneous explanation for several of the properties of the observed variability: lack of layers above the region of wave dissipation; the scale-dependent altitude of the layers; the scale-dependent magnitude of the layers; the observed altitude range of maximum variability in the ionosphere.

An exact match to an observed electron density profile with a wave model requires a careful modeling of Saturn's ionosphere (both chemistry and dynamics) and is currently underway.

Appendix

The results from the wavelet analysis of all individual Cassini electron density profiles of Saturn that are published to date are presented here in chronological order starting with S07 entry in 2005 (Fig. A.1) and finishing with S75 exit in 2008 (Fig. A.27) . The format of the plots is the same as in Fig. 1. The Discussions (Sec. 6) and the Conclusions (Sec. 7) in this paper are based on the results presented these figures.

Figures A.1 to A.27

Acknowledgments

The authors thank Dr. A. J. Kliore for providing the electron density profiles for Saturn obtained by the the Cassini Radio Science Experiment.

References

1. Barrow, D. and Matcheva, K. I., 2011. Impact of atmospheric gravity waves on the jovian ionosphere. Icarus 211, 609-622.

2. Barrow, D., Matcheva, K. I., and Drossart, P., 2012. Prospects for Observing Atmospheric Gravity Waves in Jupiter's Thermosphere Using H_3^+ Emission. Icarus, in press.

3. Conrath, B. J. and Gautier, D., 2000. Saturn Helium Abundance: A Reanalysis of Voyager Measurements. Icarus 144, Issue Icarus, pp. 124-134.

4. Festou, M. C., and Atreya, S. K., 1982. Voyager ultraviolet stellar occultation measurements of the composition and thermal profiles of the saturnian upper atmosphere. Geophys. Res. Lett. 9, 1147-1150.

5. Fischer, G., Desch, M. D., Zarka, P., Kaiser, M. L., Gurnett, D. A., Kurth, W. S., Macher, W., Rucker, H. O., Lecacheux, A., Farrell, W. M., Cecconi, B., 2006. Saturn lightning recorded by Cassini/RPWS in 2004. Icarus 183, Issue 1, 135-152.

6. Fischer, G. Gurnett, D. A., Zarka, P., Moore, L., Dyudina, U. A., 2011. Peak electron densities in Saturn's ionosphere derived from the low-frequency cutoff of Saturn lightning. Journal of Geophysical Research, Volume 116, Issue A4.

7. Fletcher, L. N., Achterberg, R. K., Greathouse, T. K., Orton, G. S., Conrath, B. J., Simon-Miller, A. A., Teanby, N., Guerlet, S., Irwin, P. G. J., Flasar, F. M., 2010. Seasonal change on Saturn from Cassini/CIRS observations, 2004-2009. Icarus 208, 337-352.

8. Hubbard, W. B.; Porco, C. C.; Hunten, D. M.; Rieke, G. H.; Rieke, M. J.; McCarthy, D. W.; Haemmerle, V.; Haller, J.; McLeod, B.; Lebofsky, L. A.; Marcialis, R.; Holberg, J. B.; Landau, R.; Carrasco, L.; Elias, J.; Buie, M. W.; Dunham, E. W.; Persson, S. E.; Boroson, T.; West, S.; French, R. G.; Harrington, J.; Elliot, J. L.; Forrest, W. J.; Pipher, J. L.; Stover, R. J.; Brahic, A.; Grenier, I., 1997. Structure of Saturn's Mesosphere from the 28 SGR Occultations. Icarus 130, 404-425.

9. Harrington, J., French, R., Matcheva, K. I., 2010. The 1998 November 14 Occultation of GSC 0622-00345 by Saturn. II. Stratospheric Thermal Profile, Power Spectrum, and Gravity Waves. The Astrophysical Journal, Volume 716, Issue 1, 404-416.

10. Hines, C.O., 1974. The upper atmosphere in motion. Geophysical Monograph Series, vol. 18. American Geophysical Union, Washington, DC.

11. Hinson, D. P., Flasar, M. F., Kliore, A. J., Schinder, P. J., Twicken, J. D., Harrera, R. G., 1997. Results from the first Galileo radio occultation experiment. J. Geophys. Res. Lett. 24, 2107-2110.

12. Kelley, M. C., 1989.The Earth's Ionosphere. Plasma Physics and Electrodynamics. Academic Press, San Diego, CA.

13. Kliore, A. J., Nagy, A. F., Marouf, E. A., Anabtawi, A., Barbinis, E., Fleischman, D. U., Kahan, D. S., 2009. Midlatitude and high-latitude electron density profiles in the ionosphere of Saturn obtained by Cassini radio occultation observations. Journal of Geophysical Research, Volume 114, Issue A4, CiteID A04315.

14. Lindal, G. F., Sweetnam, D. N., and Eshleman, V. R., 1985. The atmosphere of Saturn: An analysis of the Voyager radio occultation measurements. Astron. J. 90, 1136-1146.

15. Lindzen, R.S., 1981. Turbulence and stress owing to gravity wave and tidal breakdown. J. Geophys. Res. 86, 9707-9714.

16. Majeed, T., McConneell, J. C., 1991. The upper ionospheres of Jupiter and Saturn. Planetary and Space Science, vol. 39, 1715-1732.

17. Majeed, T., McConneell, J. C., 1996. Voyager electron density measurements on Saturn: Analysis with a time dependent ionospheric model. Journal of Geophysical Research, Volume 101, Issue E3, 7589-7598.

18. Matcheva, K. I., and Strobel D. F., 1999. Heating of Jupiter's thermosphere by dissipation of gravity waves due to molecular viscosity and heat conduction. Icarus 140, 328-340.

19. Matcheva, K. I., Strobel, D. F., Flasar, F. M., 2001. Interaction of gravity waves with ionospheric plasma: Implications for Jupiter's ionosphere. Icarus 152, 347-365.

20. Moses, J. I. and Bass, S. F., 2000. The effects of external material on the chemistry and structure of Saturn's ionosphere. Journal of Geophysical Research, Volume 105, Issue E3, 7013-7052.

21. Moses, J. I., Bezard, B., Lellouch, E., Gladstone, G.,Feuchtgruber, H., Allen, M., 2000, Photochemistry of Saturn's Atmosphere: I. Hydrocarbon Chemistry and Comparison with ISO Observations. Icarus 143, 244-298.

22. Moore, L. E., Mendillo, M., Mueller-Wodarg, I. C. F., Murr, D. L., 2004. Modeling of global variations and ring shadowing in Saturn's ionosphere. Icarus 172, 503-520.

23. Moore, L., Mueller-Wodarg, I., Galand, M., Kliore, A., Mendillo, M., 2010. Latitudinal variations in Saturn's ionosphere: Cassini measurements and model comparisons. Journal of Geophysical Research, Volume 115, Issue A11, CiteID A11317.

24. Nagy, A. F., Kliore, A. J., Marouf, E., French, R., Flasar, M., Rappaport, N. J., Anabtawi, A., Asmar, S. W., Johnston, D., Barbinis, E., Goltz, G., Fleischman, D., 2006. First results from the ionospheric radio occultations of Saturn by the Cassini spacecraft. Journal of Geophysical Research, Volume 111, Issue A6, CiteID A06310.

25. Nagy, A. , Arvydas J. Kliore, Michael Mendillo, Steve Miller, Luke Moore, Julianne I. Moses, Ingo Mueller-Wodarg, and Don Shemansky, 2009. Upper Atmosphere and Ionosphere of Saturn. in "Saturn from Cassini-Huygens", by Dougherty, Michele K.; Esposito, Larry W.; Krimigis, Stamatios M., ISBN 978-1-4020-9216-9. Springer Science Business Media B.V., p. 181.

26. Smith, G. R., Shemansky, D. E., Holberg, J. B., Broadfoot, A. L., Sandel, B. R., and McConnell, J. C., 1983. Saturn's upper atmosphere from the Voyager 2 EUV solar and stellar occultations. J. Geophys. Res. 88, 8667-8678.

27. Torrence, C. and Compo, P., 1998. A practical Guide to Wavelet Analysis. Bull. Amer. Meteor. Soc., 79, 61-78.

28. Walterscheid, R.L., 1981. Dynamical cooling induced by dissipating internal gravity waves. J. Geophys. Res. Lett. 8, 1235-1238.

29. Warwick, J. W., Evans, D. R., Romig, J. H., Alexander, J. K., Desch, M. D., Kaiser, M. L., Aubier, M. G., Leblanc, Y., Lecacheux, A., Pedersen, B. M., 1982. Planetary radio astronomy observations from Voyager 2 near Saturn. Science, vol. 215, Jan. 29, 1982, p. 582-587.

30. Warwick, J. W., Pearce, J. B., Evans, D. R., Carr, T. D., Schauble, J. J., Alexander, J. K., Kaiser, M. L., Desch, M. D., Pedersen, M., Lecacheux, A., Daigne, G., Boischot, A., Barrow, C. H., 1981. Planetary radio astronomy observations from Voyager 1 near Saturn. Science, vol. 212, Apr. 10, 1981, p. 239-243.

List of Tables:

TABLE I

Latitude	Obs.	Dawn/Dusk	S [km]	Z_{max}	$\Delta N_{e,max}$ [cm^{-3}]
72°S	S56 exit	dusk	500	500-2500 km	1000
			250	1000	2500
			165	1200	2000
28°S	S68 entry	dusk	430	1350	5000
			210	1000	2000
3°S	S08 entry	dusk	380	1250	2000
9°S	S07 exit	dawn	570	800	190
			360	1800	150

Table I: Summary of the vertical scales of variability ($S < 700$ km) identified in the electron density profiles shown in Figs. 1-4.

List of Figures and figure captions:

Figure 1: High latitude dusk observation (72°S). Left panel: Electron density profile from S56 exit radio occultation. Central panel: Electron density variations as a function of scale and altitude. Right panel: Amplitude of the variations as a function of scale and altitude. Contours (solid black lines) are drawn at 5% increments. In the right panel the light solid lines mark the height of dissipation, z_d, for gravity waves with a period 30 min (line A) and 10 hours (line B).

Figure 2: Mid latitude dusk observation (28°S). Left panel: Electron density profile from S68 entry radio occultation. Central panel: Electron density variations as a function of scale and altitude. Right panel: Amplitude of the variations as a function of scale and altitude. Contours (solid black lines) are drawn at 5% increments. In the right panel the light solid lines mark the height of dissipation, z_d, for gravity waves with a period 30 min (line A) and 10 hours (line B).

Figure 3: Low latitude dusk observation (3°S). Left panel: Electron density profile from S08 entry radio occultation. Central panel: Electron density variations as a function of scale and altitude. Right panel: Amplitude of the variations as a function of scale and altitude. Contours (solid black lines) are drawn at 5% increments. In the right panel the light solid lines mark the height of dissipation, z_d, for gravity waves with a period 30 min (line A) and 10 hours (line B).

Figure 4: Low latitude dawn observation (9°S). Left panel: electron density profile from S07 exit radio occultation. Central panel: electron density variations as a function of scale and altitude. Right panel: amplitude of the variations as a function of scale and altitude. Contours (solid black lines) are drawn at 5% increments. In the right panel the light solid lines mark the height of dissipation, z_d, for gravity waves with a period 30 min (line A) and 10 hours (line B).

Figure 5: Histogram of the number of detections of individual scales with an amplitude larger than 5%: a) all electron density profiles (31 observations); b) high latitudes only (8 observations); c) middle latitudes (7 observations) ; d) low latitudes (16 observations). The count is normalized by the number of the corresponding observations.

Figure 6: Histogram of the number of detections of individual scales with an amplitude larger than 5%: a) low latitude dawn conditions (8 observations); b) low latitude dusk conditions (8 observations).

Figure 7: Histogram of the number of detections of individual scales with an amplitude larger than 5%: a) 2005 observations (12 observation); b) late 2007- 2008 observations (14 observations)

Figure 8: Structure of the steady state neutral atmosphere.

Figure 9: Atmospheric gravity wave model. Bottom axis: wave amplitude profile (red - vertical velocity; green - horizontal velocity; blue - temperature profile). Top axis: vertical wavelength in black solid line.

Figure 10: Wave dissipation altitude. Each curve corresponds to a family of waves with the same period ranging from 30 min (top curve) period to 10 hours (bottom curve) in increments of 10 min.

APPENDIX

Figure A.1 Low latitude dusk observation (4.9°S). Left panel: Electron density profile from S07 entry radio occultation. Central panel: Electron density variations as a function of scale and altitude. Right panel: Amplitude of the variations as a function of scale and altitude. Contours (solid black lines) are drawn at 5% increments. In the right panel the light solid lines mark the height of dissipation, z_d, for gravity waves with a period 30 min

(line A) and 10 hours (line B).

Figure A.2: Low latitude dawn observation (8.3°S). Left panel: Electron density profile from S08 exit radio occultation. Central panel: Electron density variations as a function of scale and altitude. Right panel: Amplitude of the variations as a function of scale and altitude. Contours (solid black lines) are drawn at 5% increments. In the right panel the light solid lines mark the height of dissipation, z_d, for gravity waves with a period 30 min (line A) and 10 hours (line B).

Figure A.3: Low latitude dawn observation (7.4°S). Left panel: Electron density profile from S09 exit radio occultation. Central panel: Electron density variations as a function of scale and altitude. Right panel: Amplitude of the variations as a function of scale and altitude. Contours (solid black lines) are drawn at 10% increments starting at 5%. In the right panel the light solid lines mark the height of dissipation, z_d, for gravity waves with a period 30 min (line A) and 10 hours (line B).

Figure A.4: Low latitude dusk observation (1.6°N). Left panel: Electron density profile from S10 entry radio occultation. Central panel: Electron density variations as a function of scale and altitude. Right panel: Amplitude of the variations as a function of scale and altitude. Contours (solid black lines) are drawn at 5% increments. In the right panel the light solid lines mark the height of dissipation, z_d, for gravity waves with a period 30 min (line A) and 10 hours (line B).

Figure A.5: Low latitude dawn observation (6.1°S). Left panel: Electron density profile from S10 exit radio occultation. Central panel: Electron density variations as a function of scale and altitude. Right panel: Amplitude of the variations as a function of scale and altitude. Contours (solid black lines) are drawn at 5% increments. In the right panel the light solid lines mark the height of dissipation, z_d, for gravity waves with a period 30 min (line A) and 10 hours (line B).

Figure A.6: Low latitude dawn observation (4.5°S). Left panel: Electron density profile from S11 exit radio occultation. Central panel: Electron density variations as a function of scale and altitude. Right panel: Amplitude of the variations as a function of scale and altitude. Contours (solid black lines) are drawn at 5% increments. In the right panel the light solid lines mark the height of dissipation, z_d, for gravity waves with a period 30 min (line A) and 10 hours (line B).

Figure A.7: Low latitude dusk observation (7.5°N). Left panel: Electron density profile from S12 entry radio occultation. Central panel: Electron density variations as a function of scale and altitude. Right panel: Amplitude of the variations as a function of scale and altitude. Contours (solid black lines) are drawn at 5% increments. In the right panel the light solid lines mark the height of dissipation, z_d, for gravity waves with a period 30 min (line A) and 10 hours (line B).

Figure A.8: Low latitude dawn observation (2.6°S). Left panel: Electron density profile from S12 exit radio occultation. Central panel: Electron density variations as a function of scale and altitude. Right panel: Amplitude of the variations as a function of scale and altitude. Contours (solid black lines) are drawn at 5% increments. In the right panel the light solid lines mark the height of dissipation, z_d, for gravity waves with a period 30 min (line A) and 10 hours (line B).

Figure A.9: Low latitude dawn observation (0.5°S). Left panel: Electron density profile from S13 exit radio occultation. Central panel: Electron density variations as a function of scale and altitude. Right panel: Amplitude of the variations as a function of scale and altitude. Contours (solid black lines) are drawn at 5% increments. In the right panel the light solid lines mark the height of dissipation, z_d, for gravity waves with a period 30 min (line A) and 10 hours (line B).

Figure A.10: Low latitude dusk observation (8.4°S). Left panel: Electron density profile from S14 entry radio occultation. Central panel: Electron density variations as a function

of scale and altitude. Right panel: Amplitude of the variations as a function of scale and altitude. Contours (solid black lines) are drawn at 5% increments. In the right panel the light solid lines mark the height of dissipation, z_d, for gravity waves with a period 30 min (line A) and 10 hours (line B).

Figure A.11: Low latitude dusk observation (5.0°S). Left panel: Electron density profile from S28 entry radio occultation. Central panel: Electron density variations as a function of scale and altitude. Right panel: Amplitude of the variations as a function of scale and altitude. Contours (solid black lines) are drawn at 5% increments. In the right panel the light solid lines mark the height of dissipation, z_d, for gravity waves with a period 30 min (line A) and 10 hours (line B).

Figure A.12: High latitude observation (75.4°N). Left panel: Electron density profile from S44 entry radio occultation. Central panel: Electron density variations as a function of scale and altitude. Right panel: Amplitude of the variations as a function of scale and altitude. Contours (solid black lines) are drawn at 5% increments. In the right panel the light solid lines mark the height of dissipation, z_d, for gravity waves with a period 30 min (line A) and 10 hours (line B).

Figure A.13: Low latitude dawn observation (3.2°S). Left panel: Electron density profile from S44 exit radio occultation. Central panel: Electron density variations as a function of scale and altitude. Right panel: Amplitude of the variations as a function of scale and altitude. Contours (solid black lines) are drawn at 5% increments. In the right panel the light solid lines mark the height of dissipation, z_d, for gravity waves with a period 30 min (line A) and 10 hours (line B).

Figure A.14: Low latitude dusk observation (5.0°S). Left panel: Electron density profile from S46 exit radio occultation. Central panel: Electron density variations as a function of scale and altitude. Right panel: Amplitude of the variations as a function of scale and altitude. Contours (solid black lines) are drawn at 5% increments. In the right panel the

light solid lines mark the height of dissipation, z_d, for gravity waves with a period 30 min (line A) and 10 hours (line B).

Figure A.15: Middle latitude dawn observation (41.2°N). Left panel: Electron density profile from S47 exit radio occultation. Central panel: Electron density variations as a function of scale and altitude. Right panel: Amplitude of the variations as a function of scale and altitude. Contours (solid black lines) are drawn at 5% increments. In the right panel the light solid lines mark the height of dissipation, z_d, for gravity waves with a period 30 min (line A) and 10 hours (line B).

Figure A.16: Middle latitude dusk observation (38.7°S). Left panel: Electron density profile from S51 entry radio occultation. Central panel: Electron density variations as a function of scale and altitude. Right panel: Amplitude of the variations as a function of scale and altitude. Contours (solid black lines) are drawn at 5% increments. In the right panel the light solid lines mark the height of dissipation, z_d, for gravity waves with a period 30 min (line A) and 10 hours (line B).

Figure A.17: Middle latitude dawn observation (43.6°S). Left panel: Electron density profile from S51 exit radio occultation. Central panel: Electron density variations as a function of scale and altitude. Right panel: Amplitude of the variations as a function of scale and altitude. Contours (solid black lines) are drawn at 5% increments. In the right panel the light solid lines mark the height of dissipation, z_d, for gravity waves with a period 30 min (line A) and 10 hours (line B).

Figure A.18: Low latitude dusk observation (17.9°S). Left panel: Electron density profile from S54 entry radio occultation. Central panel: Electron density variations as a function of scale and altitude. Right panel: Amplitude of the variations as a function of scale and altitude. Contours (solid black lines) are drawn at 5% increments. In the right panel the light solid lines mark the height of dissipation, z_d, for gravity waves with a period 30 min (line A) and 10 hours (line B).

Figure A.19: High latitude observation (68.7°S). Left panel: Electron density profile from S54 exit radio occultation. Central panel: Electron density variations as a function of scale and altitude. Right panel: Amplitude of the variations as a function of scale and altitude. Contours (solid black lines) are drawn at 5% increments. In the right panel the light solid lines mark the height of dissipation, z_d, for gravity waves with a period 30 min (line A) and 10 hours (line B).

Figure A.20: High latitude observation (74.1°S). Left panel: Electron density profile from S58 exit radio occultation. Central panel: Electron density variations as a function of scale and altitude. Right panel: Amplitude of the variations as a function of scale and altitude. Contours (solid black lines) are drawn at 5% increments. In the right panel the light solid lines mark the height of dissipation, z_d, for gravity waves with a period 30 min (line A) and 10 hours (line B).

Figure A.21: High latitude observation (65.6°S). Left panel: Electron density profile from S68 exit radio occultation. Central panel: Electron density variations as a function of scale and altitude. Right panel: Amplitude of the variations as a function of scale and altitude. Contours (solid black lines) are drawn at 5% increments. In the right panel the light solid lines mark the height of dissipation, z_d, for gravity waves with a period 30 min (line A) and 10 hours (line B).

Figure A.22: Middle latitude dusk observation (42.3°S). Left panel: Electron density profile from S70 entry radio occultation. Central panel: Electron density variations as a function of scale and altitude. Right panel: Amplitude of the variations as a function of scale and altitude. Contours (solid black lines) are drawn at 5% increments. In the right panel the light solid lines mark the height of dissipation, z_d, for gravity waves with a period 30 min (line A) and 10 hours (line B).

Figure A.23: High latitude observation (69.1°S). Left panel: Electron density profile from S70 exit radio occultation. Central panel: Electron density variations as a function of scale and altitude. Right panel: Amplitude of the variations as a function of scale and altitude. Contours (solid black lines) are drawn at 5% increments. In the right panel the light solid lines mark the height of dissipation, z_d, for gravity waves with a period 30 min (line A) and 10 hours (line B).

Figure A.24: Middle latitude dusk observation (40.5°N). Left panel: Electron density profile from S72 entry radio occultation. Central panel: Electron density variations as a function of scale and altitude. Right panel: Amplitude of the variations as a function of scale and altitude. Contours (solid black lines) are drawn at 5% increments. In the right panel the light solid lines mark the height of dissipation, z_d, for gravity waves with a period 30 min (line A) and 10 hours (line B).

Figure A.25: High latitude observation (66.1°S). Left panel: Electron density profile from S72 exit radio occultation. Central panel: Electron density variations as a function of scale and altitude. Right panel: Amplitude of the variations as a function of scale and altitude. Contours (solid black lines) are drawn at 5% increments. In the right panel the light solid lines mark the height of dissipation, z_d, for gravity waves with a period 30 min (line A) and 10 hours (line B).

Figure A.26: Middle latitude dusk observation (34.2°N). Left panel: Electron density profile from S75 entry radio occultation. Central panel: Electron density variations as a function of scale and altitude. Right panel: Amplitude of the variations as a function of scale and altitude. Contours (solid black lines) are drawn at 5% increments. In the right panel the light solid lines mark the height of dissipation, z_d, for gravity waves with a period 30 min (line A) and 10 hours (line B).

Figure A.27: High latitude observation (61.8°S). Left panel: Electron density profile from S75 exit radio occultation. Central panel: Electron density variations as a function

of scale and altitude. Right panel: Amplitude of the variations as a function of scale and altitude. Contours (solid black lines) are drawn at 5% increments. In the right panel the light solid lines mark the height of dissipation, z_d, for gravity waves with a period 30 min (line A) and 10 hours (line B).

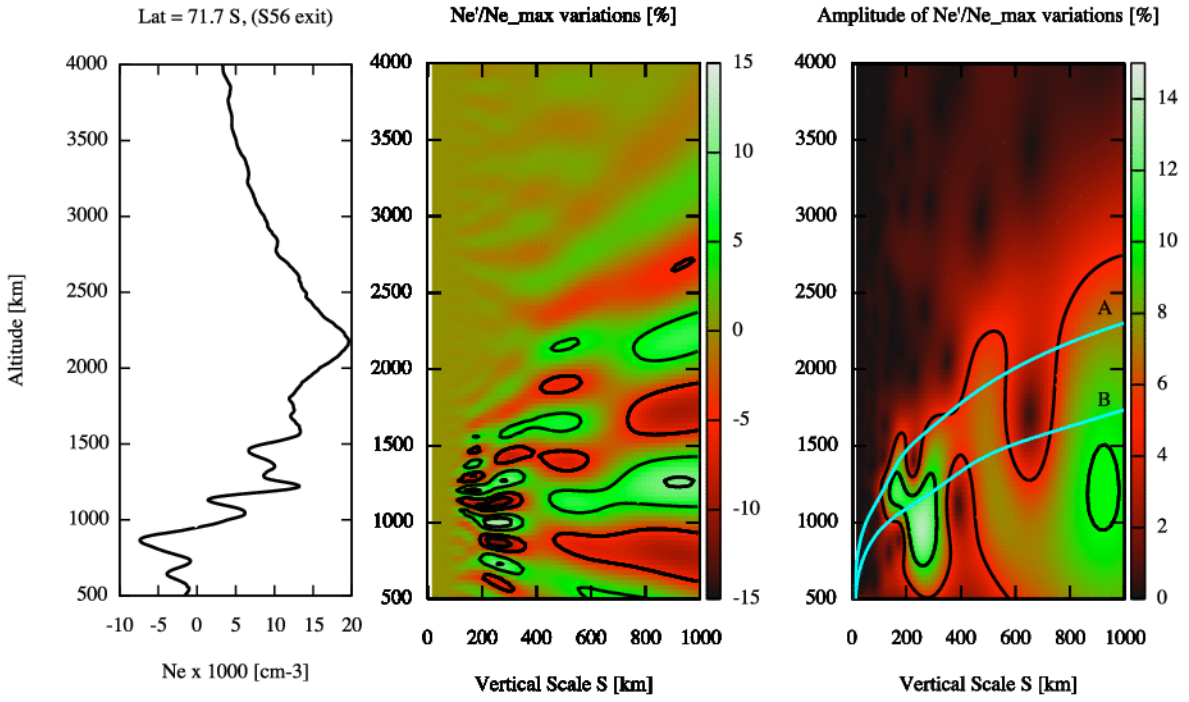

Figure 1: High latitude dusk observation (72°S). Left panel: Electron density profile from S56 exit radio occultation. Central panel: Electron density variations as a function of scale and altitude. Right panel: Amplitude of the variations as a function of scale and altitude. Contours (solid black lines) are drawn at 5% increments. In the right panel the light solid lines mark the height of dissipation, z_d, for gravity waves with a period 30 min (line A) and 10 hours (line B).

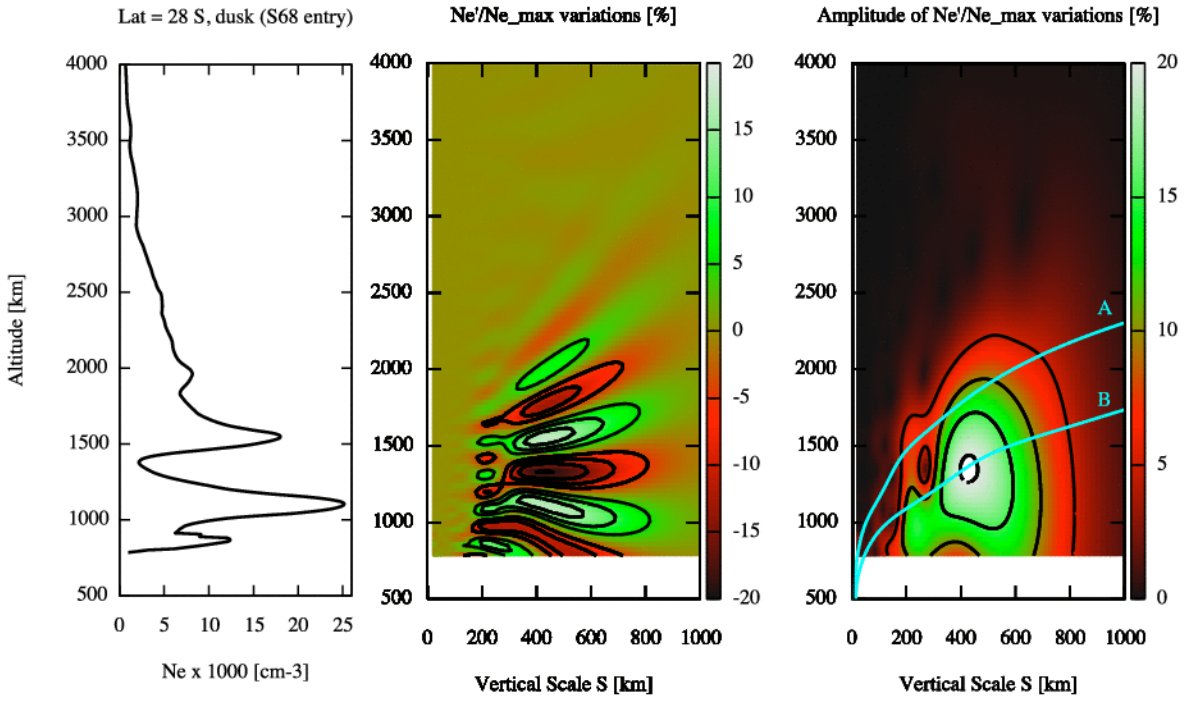

Figure 2: Mid latitude dusk observation (28°S). Left panel: Electron density profile from S68 entry radio occultation. Central panel: Electron density variations as a function of scale and altitude. Right panel: Amplitude of the variations as a function of scale and altitude. Contours (solid black lines) are drawn at 5% increments. In the right panel the light solid lines mark the height of dissipation, z_d, for gravity waves with a period 30 min (line A) and 10 hours (line B).

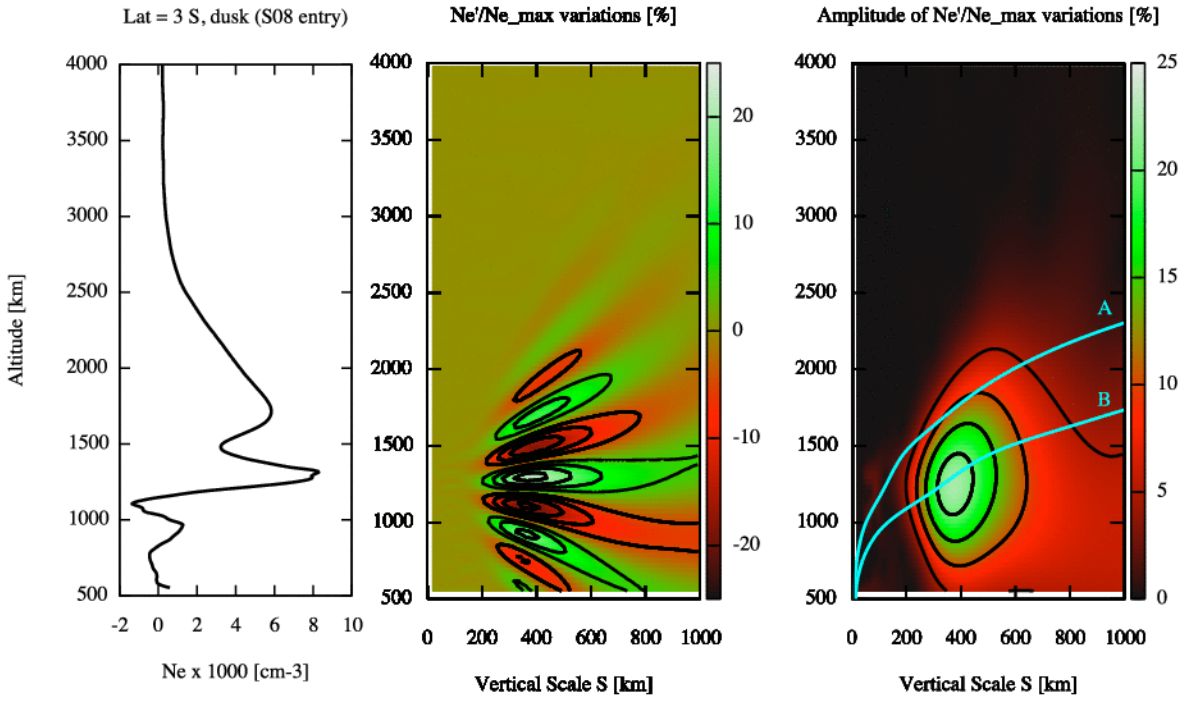

Figure 3: Low latitude dusk observation (3°S). Left panel: Electron density profile from S08 entry radio occultation. Central panel: Electron density variations as a function of scale and altitude. Right panel: Amplitude of the variations as a function of scale and altitude. Contours (solid black lines) are drawn at 5% increments. In the right panel the light solid lines mark the height of dissipation, z_d, for gravity waves with a period 30 min (line A) and 10 hours (line B).

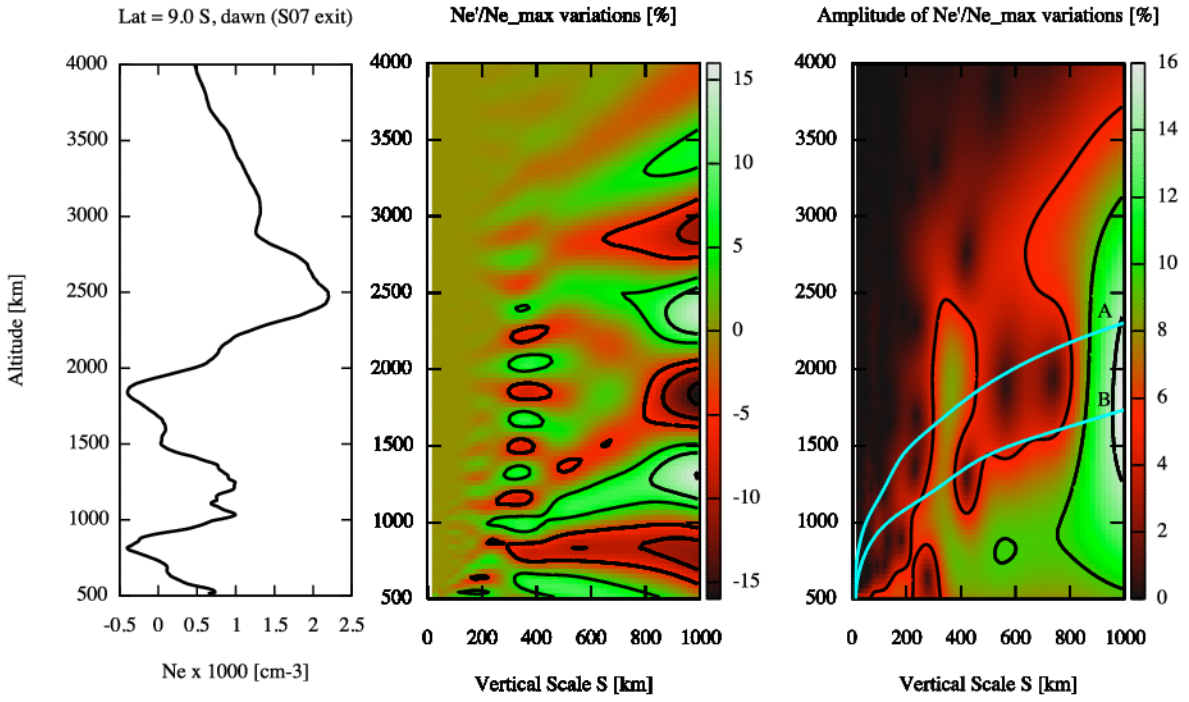

Figure 4: Low latitude dawn observation (9°S). Left panel: electron density profile from S07 exit radio occultation. Central panel: electron density variations as a function of scale and altitude. Right panel: amplitude of the variations as a function of scale and altitude. Contours (solid black lines) are drawn at 5% increments. In the right panel the light solid lines mark the height of dissipation, z_d, for gravity waves with a period 30 min (line A) and 10 hours (line B).

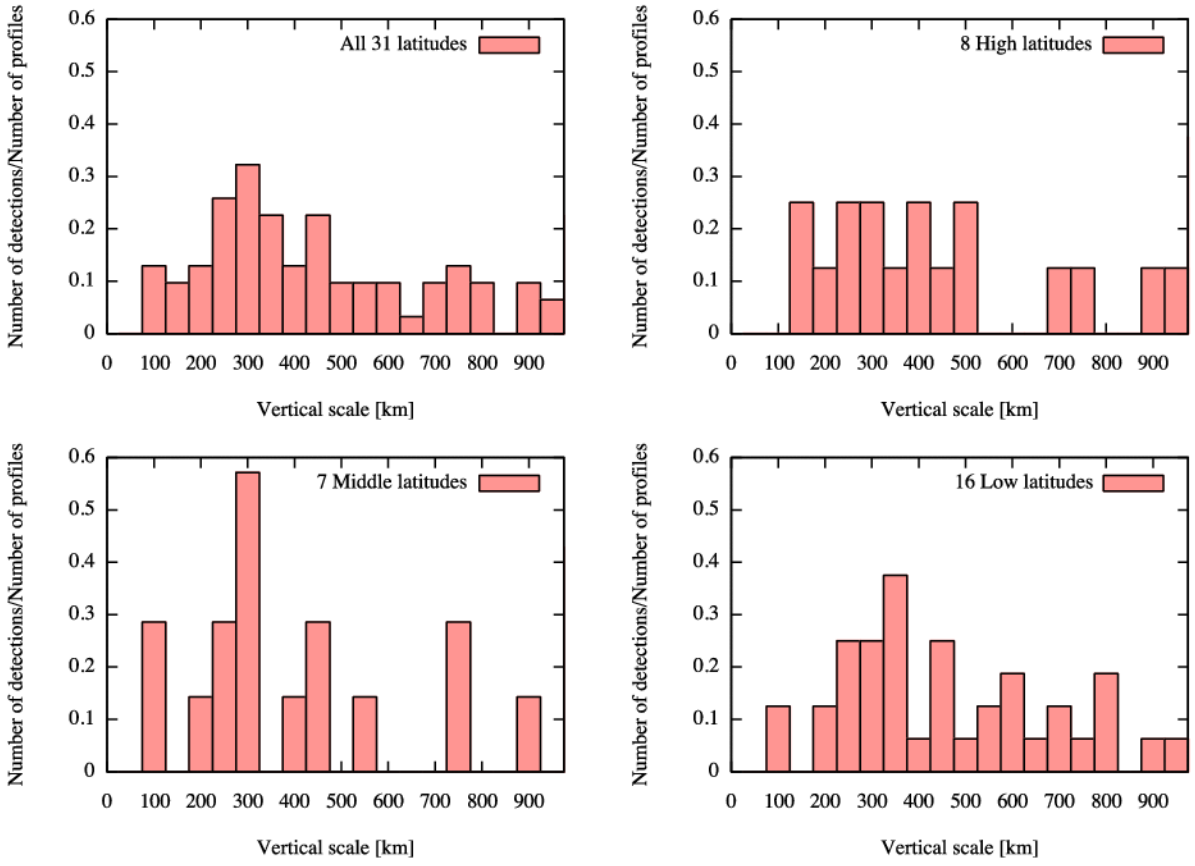

Figure 5: Histogram of the number of detections of individual scales with an amplitude larger than 5%: a) all electron density profiles (31 observations); b) high latitudes only (8 observations); c) middle latitudes (7 observations) ; d) low latitudes (16 observations). The count is normalized by the number of the corresponding observations.

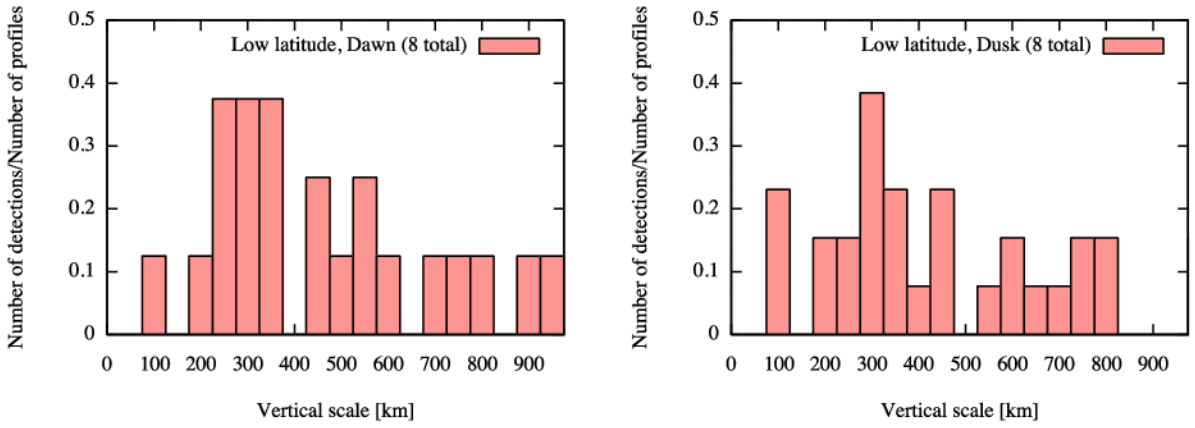

Figure 6: Histogram of the number of detections of individual scales with an amplitude larger than 5%: a) low latitude dawn conditions (8 observations); b) low latitude dusk conditions (8 observations).

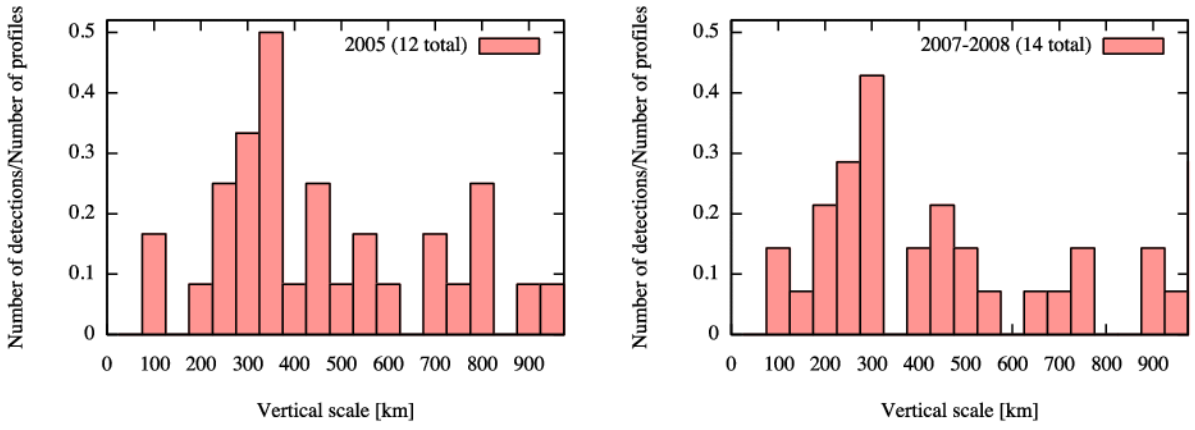

Figure 7: Histogram of the number of detections of individual scales with an amplitude larger than 5% at all latitudes: a) observations during 2005 (12 observations); b) observations during 2007-2008 (14 observations).

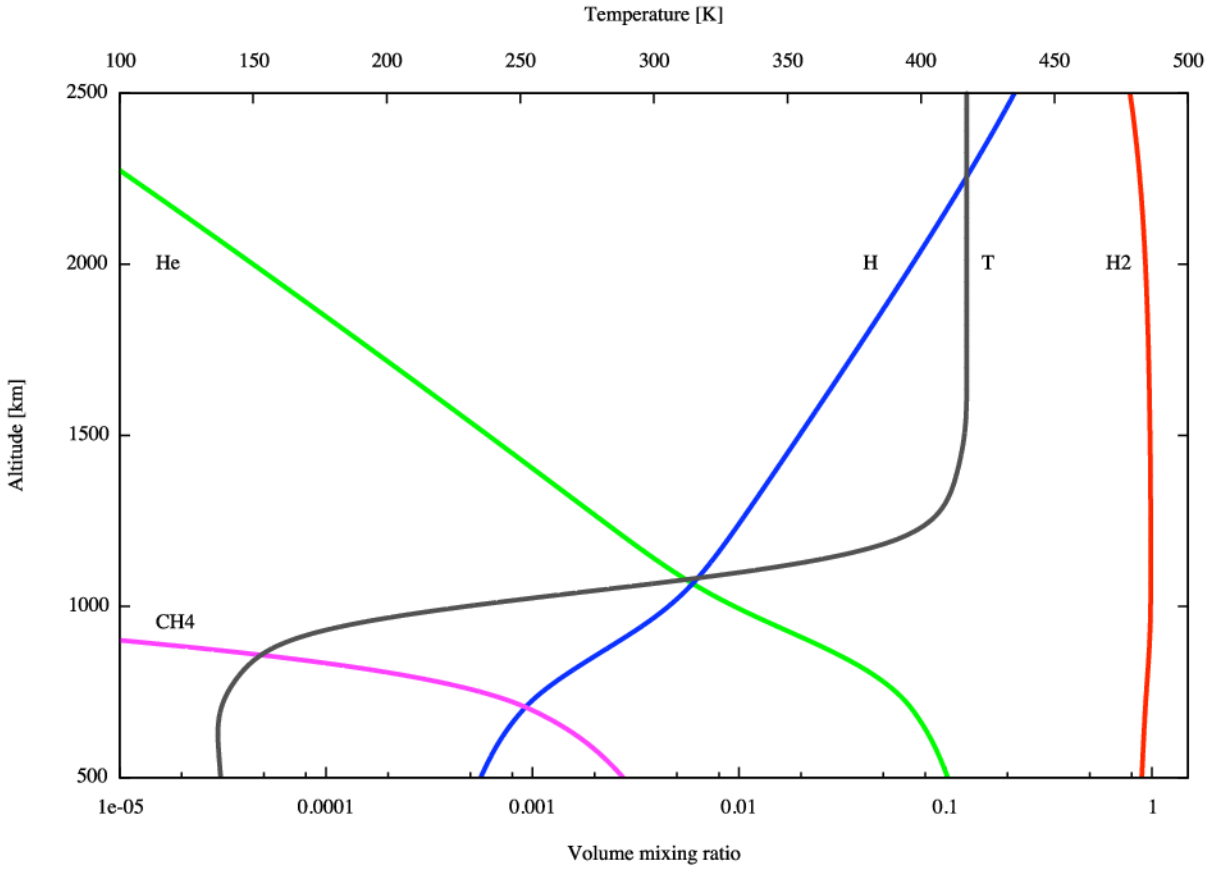

Figure 8: Structure of the steady state neutral atmosphere.

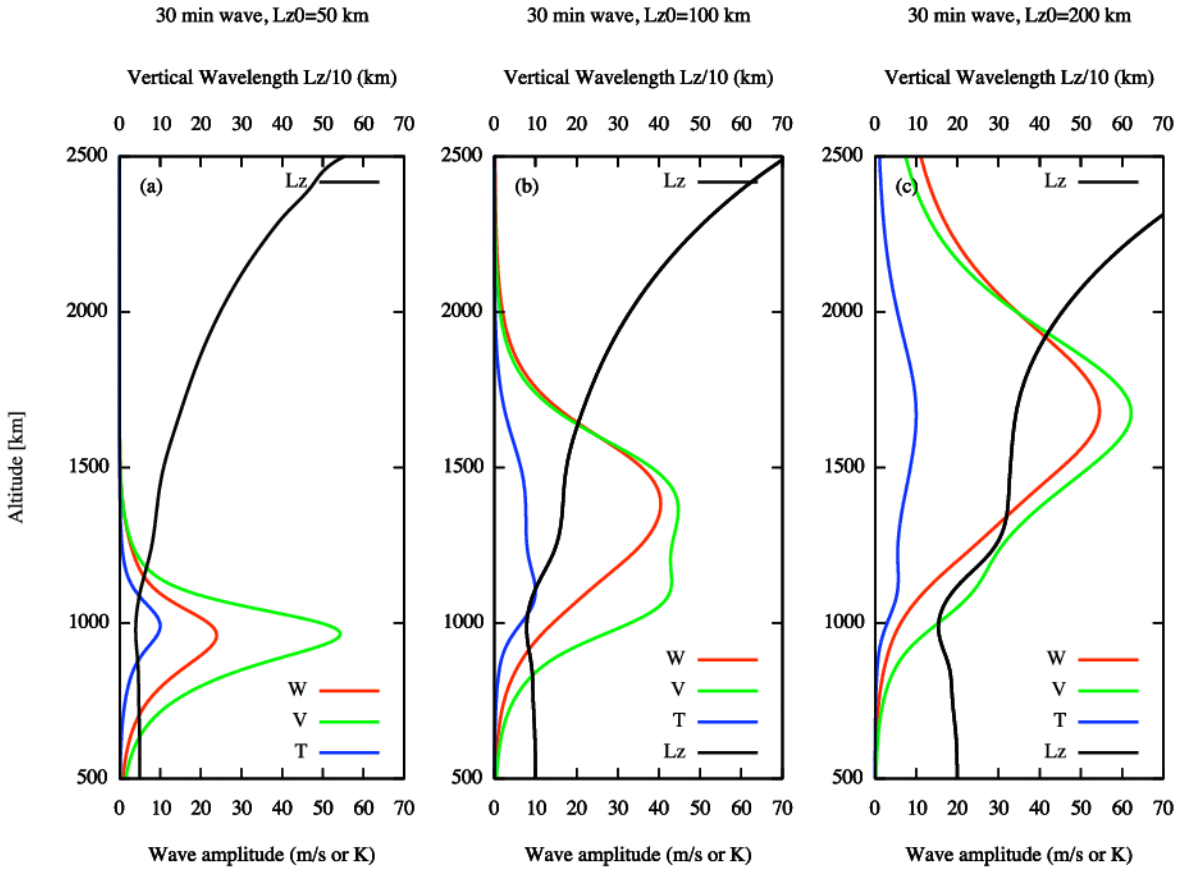

Figure 9: Atmospheric gravity wave model. Bottom axis: wave amplitude profile (red - vertical velocity; green - horizontal velocity; blue - temperature profile). Top axis: vertical wavelength in black solid line.

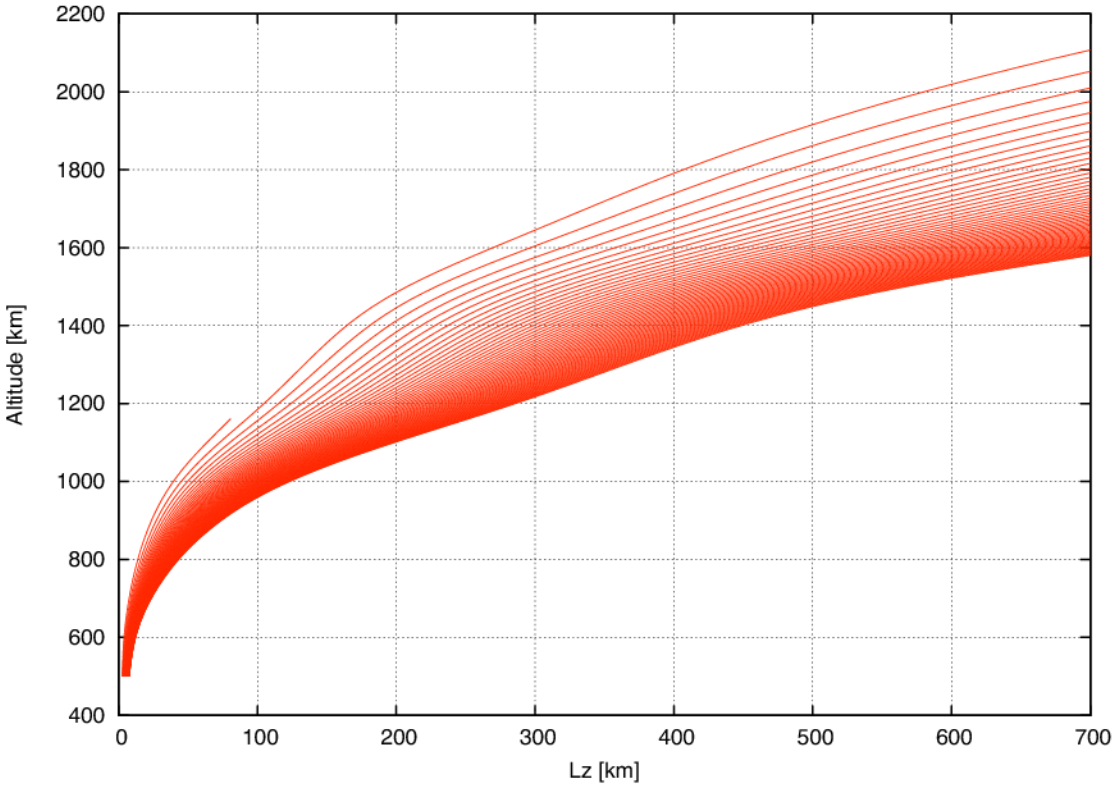

Figure 10: Wave dissipation altitude. Each curve corresponds to a family of waves with the same period ranging from 30 min (top curve) period to 10 hours (bottom curve) in increments of 10 min.

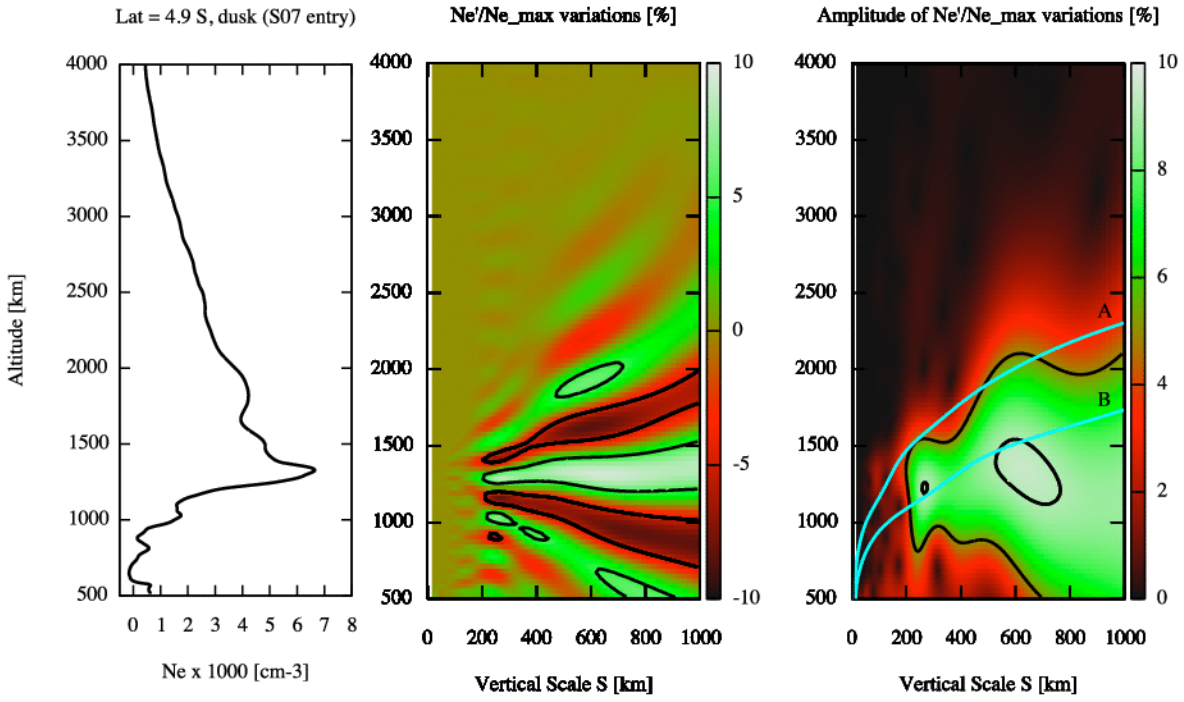

Figure A.1: Low latitude dusk observation (4.9°S). Left panel: Electron density profile from S07 entry radio occultation. Central panel: Electron density variations as a function of scale and altitude. Right panel: Amplitude of the variations as a function of scale and altitude. Contours (solid black lines) are drawn at 5% increments. In the right panel the light solid lines mark the height of dissipation, z_d, for gravity waves with a period 30 min (line A) and 10 hours (line B).

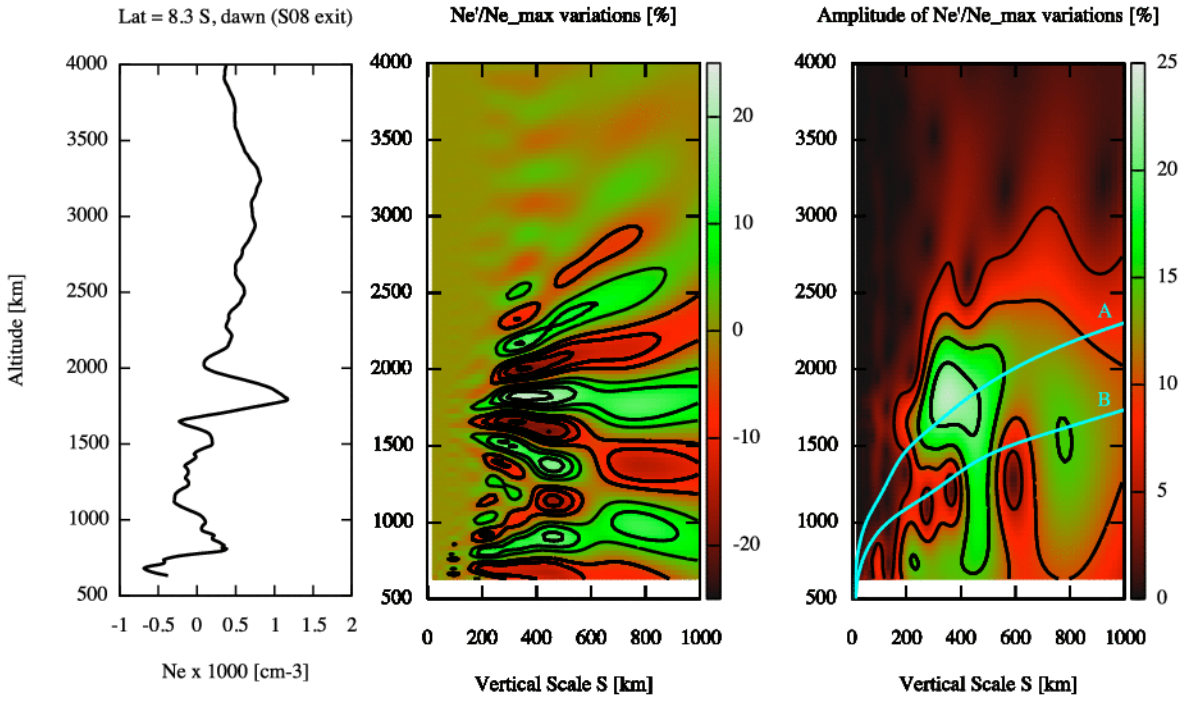

Figure A.2: Low latitude dawn observation (8.3°S). Left panel: Electron density profile from S08 exit radio occultation. Central panel: Electron density variations as a function of scale and altitude. Right panel: Amplitude of the variations as a function of scale and altitude. Contours (solid black lines) are drawn at 5% increments. In the right panel the light solid lines mark the height of dissipation, z_d, for gravity waves with a period 30 min (line A) and 10 hours (line B).

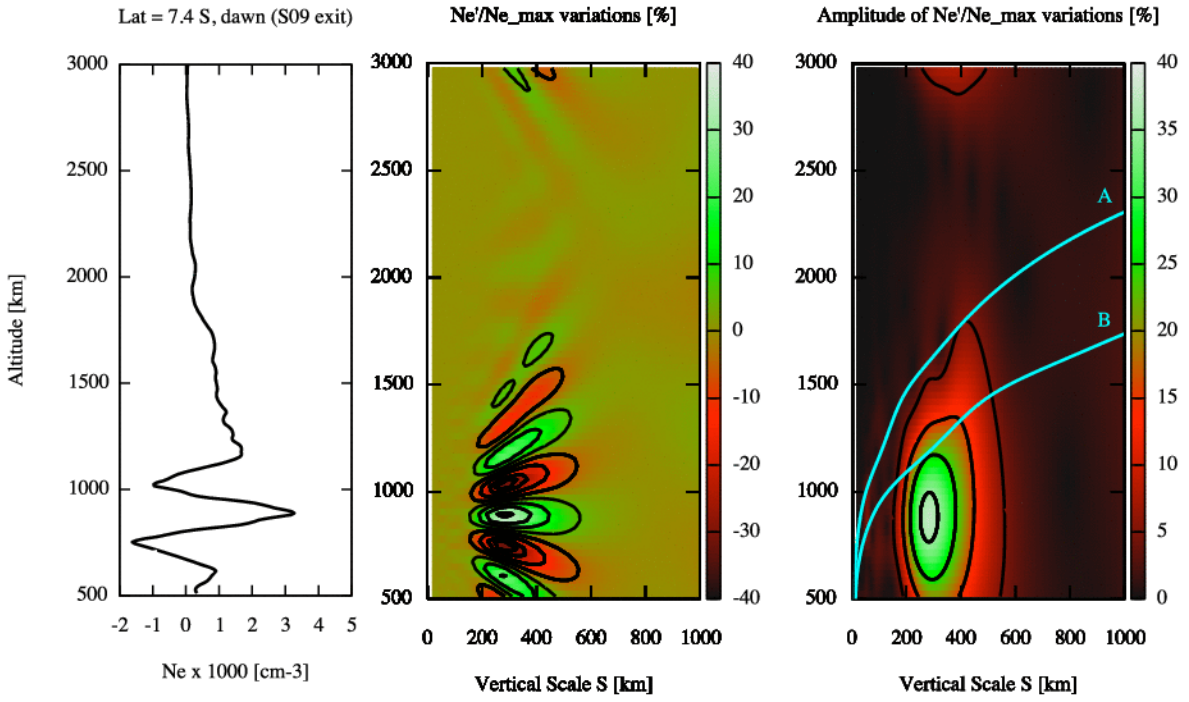

Figure A.3: Low latitude dawn observation (7.4°S). Left panel: Electron density profile from S09 exit radio occultation. Central panel: Electron density variations as a function of scale and altitude. Right panel: Amplitude of the variations as a function of scale and altitude. Contours (solid black lines) are drawn at 10% increments starting at 5%. In the right panel the light solid lines mark the height of dissipation, z_d, for gravity waves with a period 30 min (line A) and 10 hours (line B).

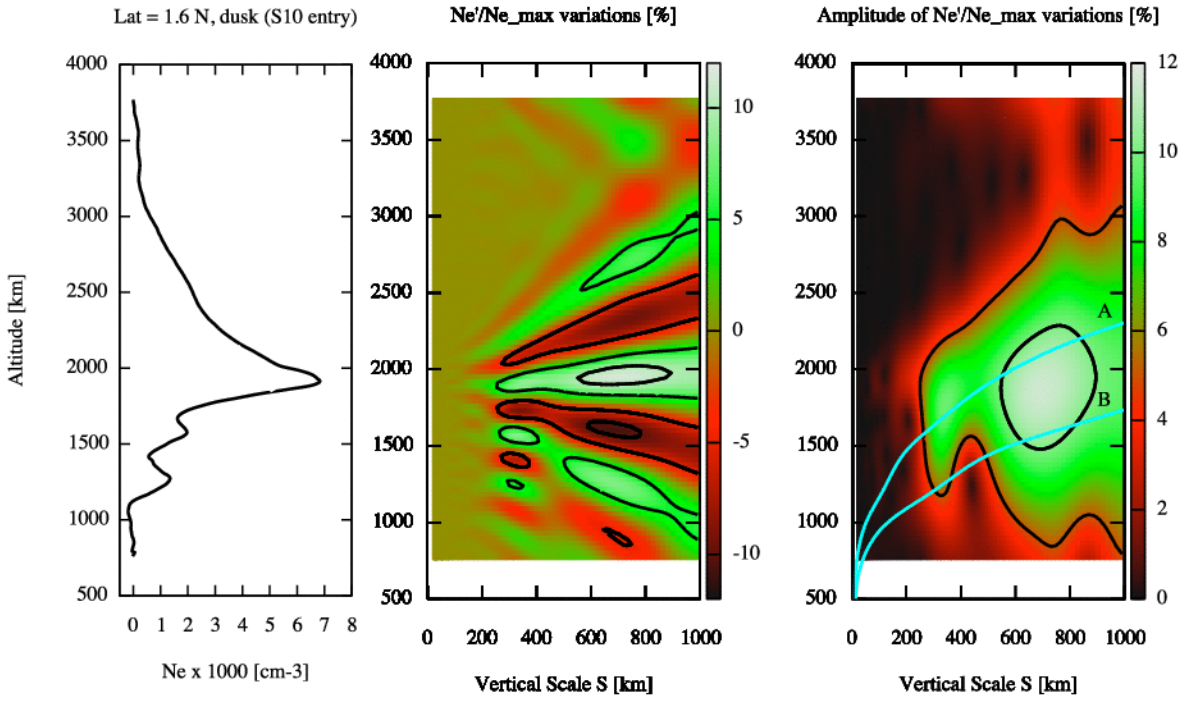

Figure A.4: Low latitude dusk observation (1.6°N). Left panel: Electron density profile from S10 entry radio occultation. Central panel: Electron density variations as a function of scale and altitude. Right panel: Amplitude of the variations as a function of scale and altitude. Contours (solid black lines) are drawn at 5% increments. In the right panel the light solid lines mark the height of dissipation, z_d, for gravity waves with a period 30 min (line A) and 10 hours (line B).

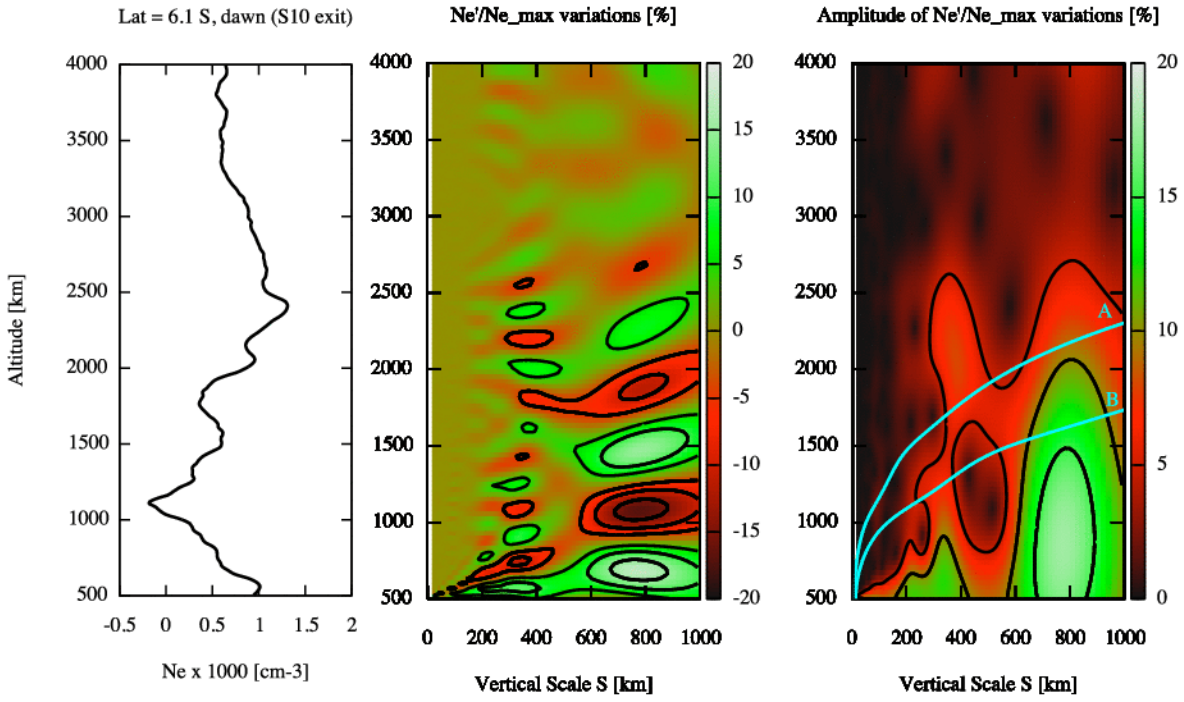

Figure A.5: Low latitude dawn observation (6.1°S). Left panel: Electron density profile from S10 exit radio occultation. Central panel: Electron density variations as a function of scale and altitude. Right panel: Amplitude of the variations as a function of scale and altitude. Contours (solid black lines) are drawn at 5% increments. In the right panel the light solid lines mark the height of dissipation, z_d, for gravity waves with a period 30 min (line A) and 10 hours (line B).

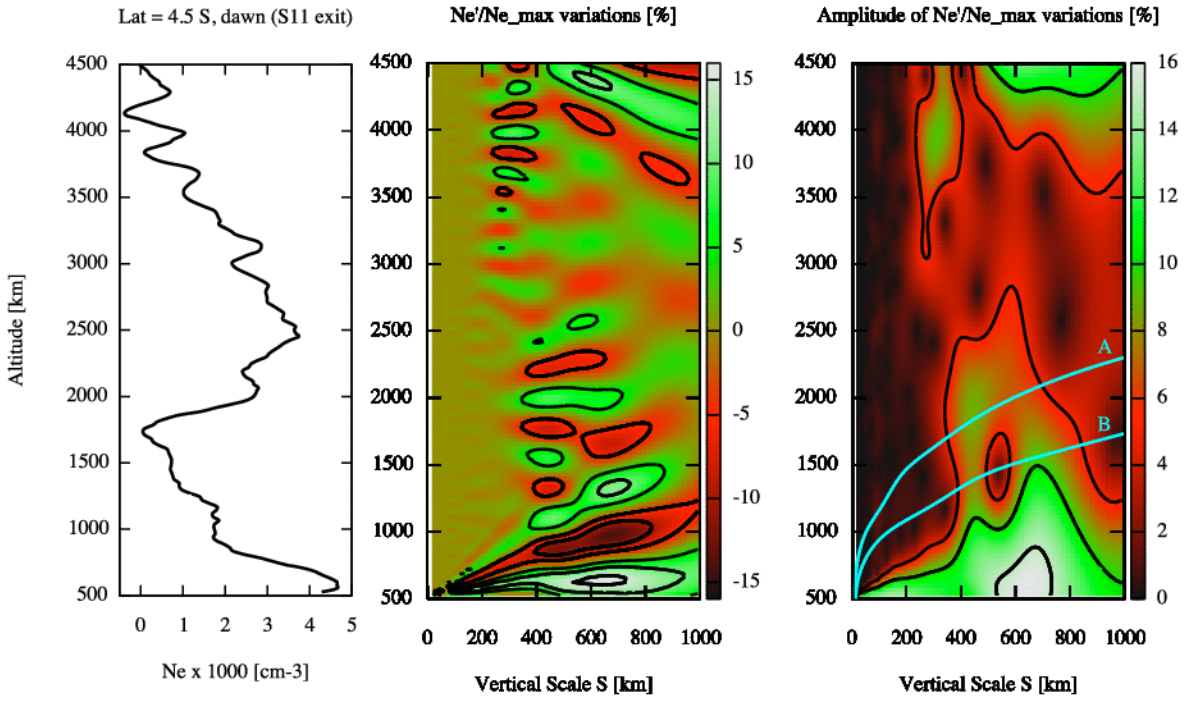

Figure A.6: Low latitude dawn observation (4.5°S). Left panel: Electron density profile from S11 exit radio occultation. Central panel: Electron density variations as a function of scale and altitude. Right panel: Amplitude of the variations as a function of scale and altitude. Contours (solid black lines) are drawn at 5% increments. In the right panel the light solid lines mark the height of dissipation, z_d, for gravity waves with a period 30 min (line A) and 10 hours (line B).

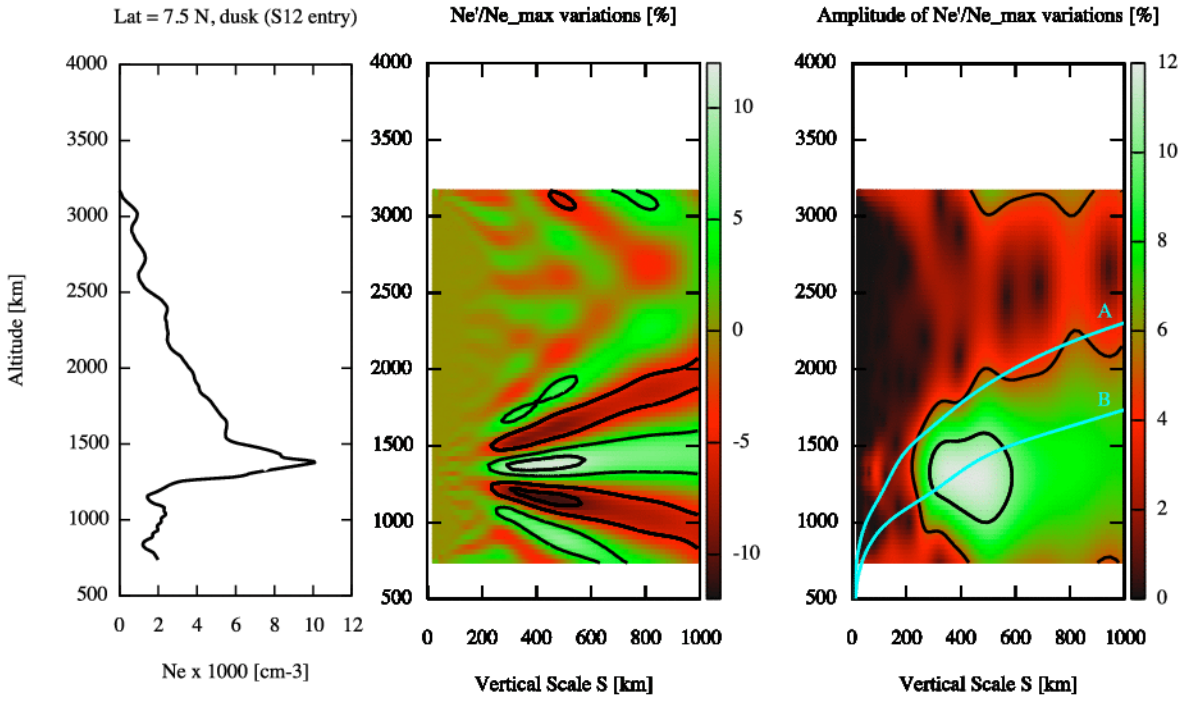

Figure A.7: Low latitude dusk observation (7.5°N). Left panel: Electron density profile from S12 entry radio occultation. Central panel: Electron density variations as a function of scale and altitude. Right panel: Amplitude of the variations as a function of scale and altitude. Contours (solid black lines) are drawn at 5% increments. In the right panel the light solid lines mark the height of dissipation, z_d, for gravity waves with a period 30 min (line A) and 10 hours (line B).

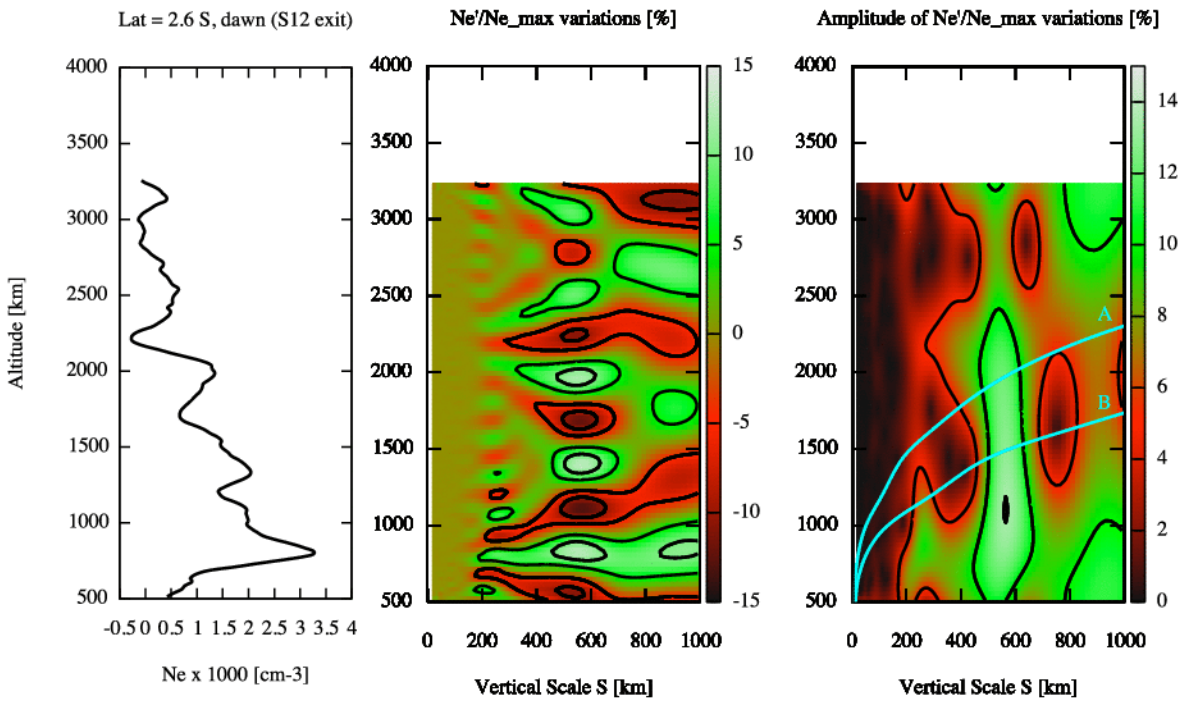

Figure A.8: Low latitude dawn observation (2.6°S). Left panel: Electron density profile from S12 exit radio occultation. Central panel: Electron density variations as a function of scale and altitude. Right panel: Amplitude of the variations as a function of scale and altitude. Contours (solid black lines) are drawn at 5% increments. In the right panel the light solid lines mark the height of dissipation, z_d, for gravity waves with a period 30 min (line A) and 10 hours (line B).

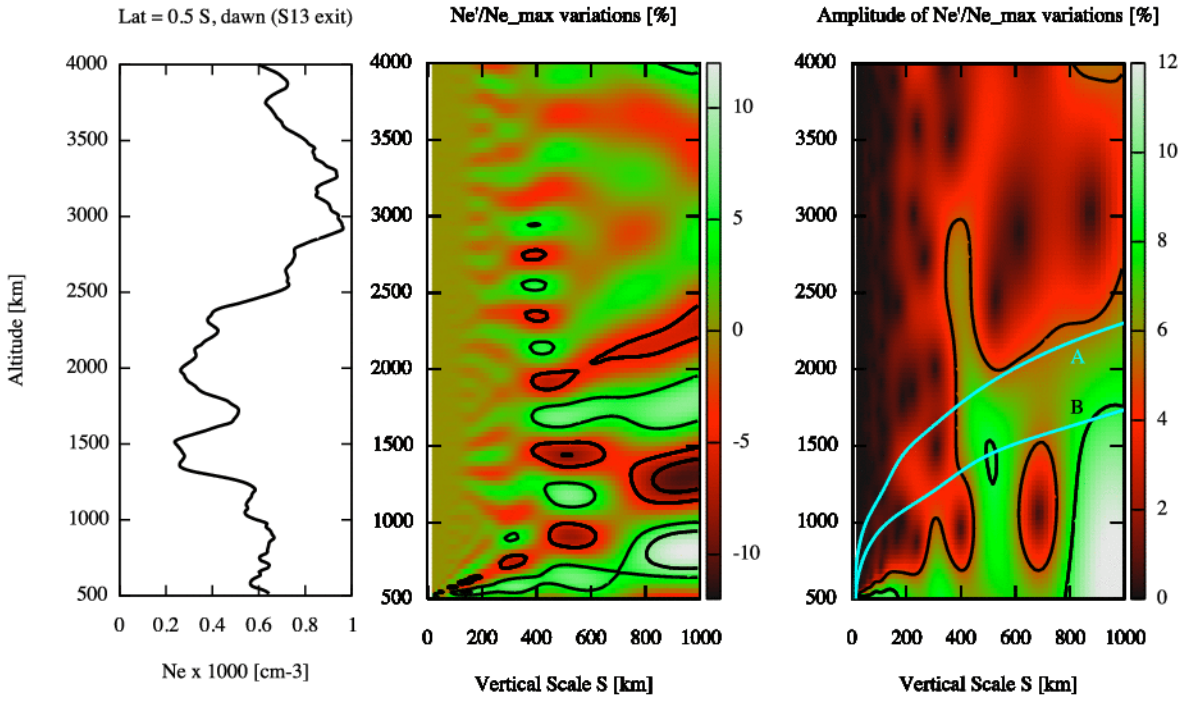

Figure A.9: Low latitude dawn observation (0.5°S). Left panel: Electron density profile from S13 exit radio occultation. Central panel: Electron density variations as a function of scale and altitude. Right panel: Amplitude of the variations as a function of scale and altitude. Contours (solid black lines) are drawn at 5% increments. In the right panel the light solid lines mark the height of dissipation, z_d, for gravity waves with a period 30 min (line A) and 10 hours (line B).

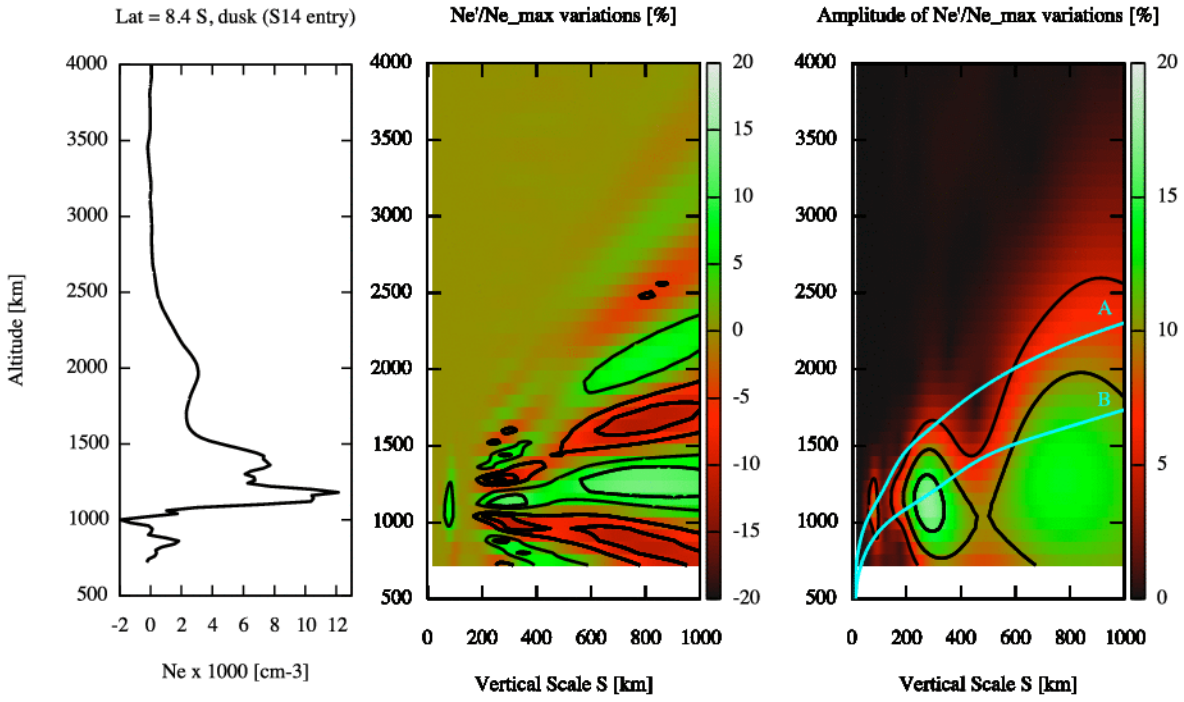

Figure A.10: Low latitude dusk observation (8.4°S). Left panel: Electron density profile from S14 entry radio occultation. Central panel: Electron density variations as a function of scale and altitude. Right panel: Amplitude of the variations as a function of scale and altitude. Contours (solid black lines) are drawn at 5% increments. In the right panel the light solid lines mark the height of dissipation, z_d, for gravity waves with a period 30 min (line A) and 10 hours (line B).

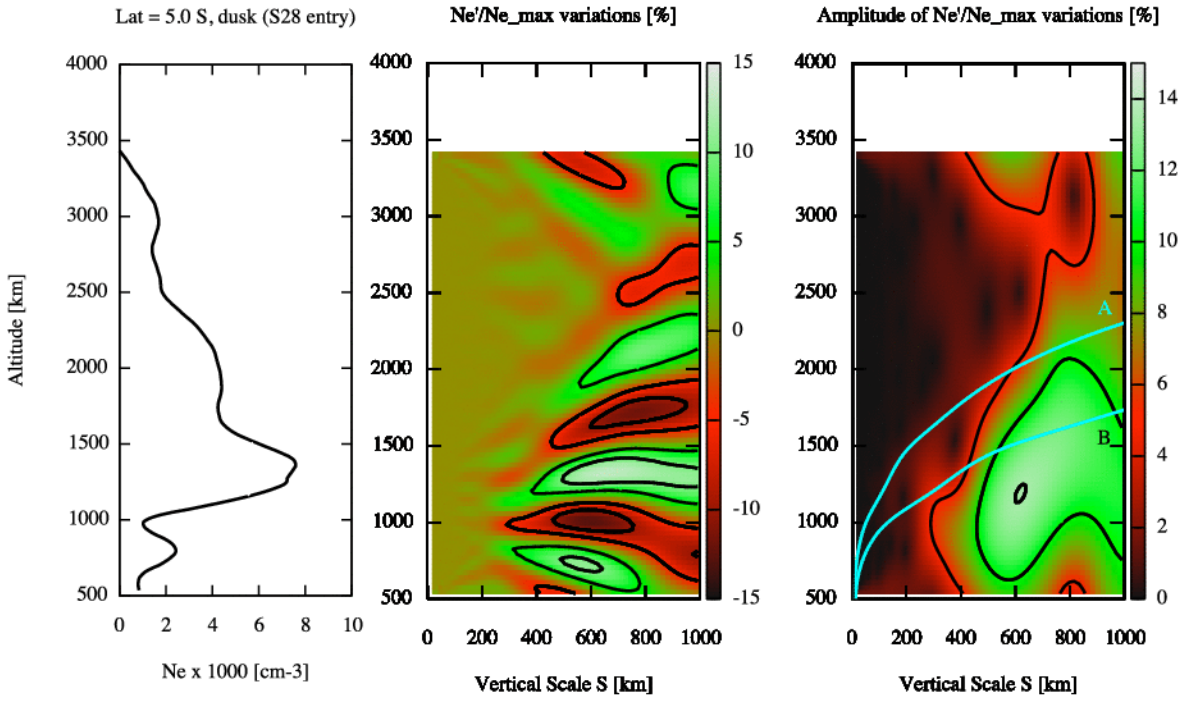

Figure A.11: Low latitude dusk observation (5.0°S). Left panel: Electron density profile from S28 entry radio occultation. Central panel: Electron density variations as a function of scale and altitude. Right panel: Amplitude of the variations as a function of scale and altitude. Contours (solid black lines) are drawn at 5% increments. In the right panel the light solid lines mark the height of dissipation, z_d, for gravity waves with a period 30 min (line A) and 10 hours (line B).

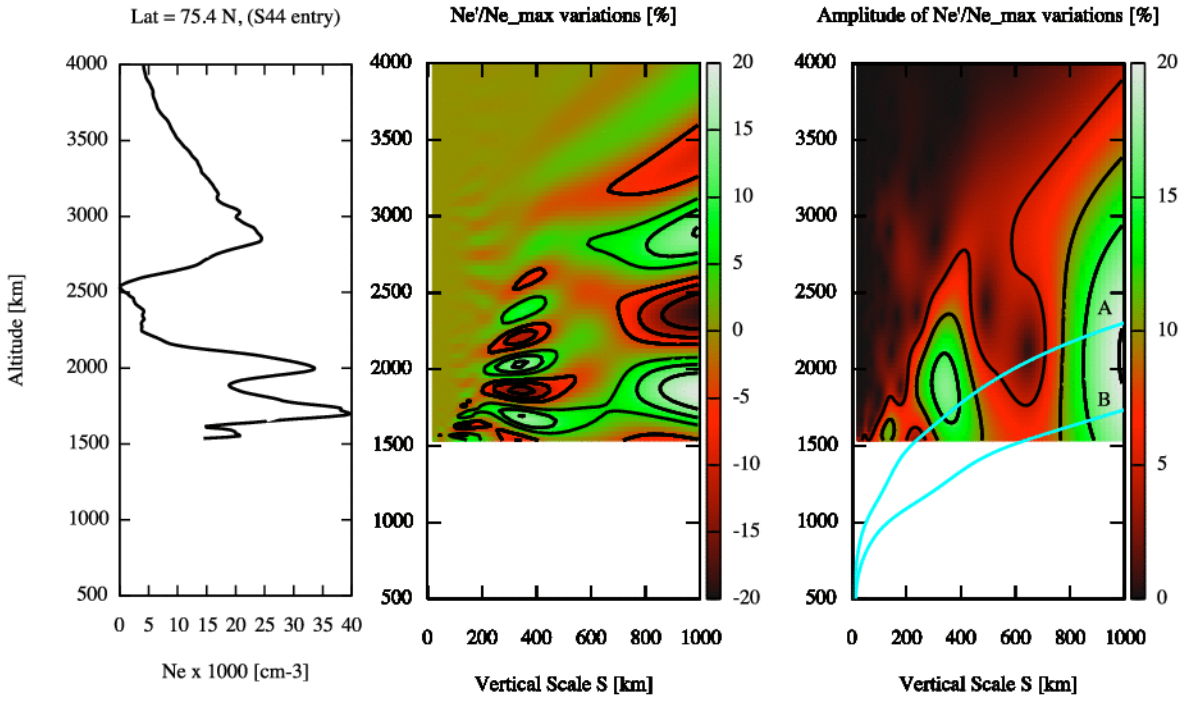

Figure A.12: High latitude observation (75.4°N). Left panel: Electron density profile from S44 entry radio occultation. Central panel: Electron density variations as a function of scale and altitude. Right panel: Amplitude of the variations as a function of scale and altitude. Contours (solid black lines) are drawn at 5% increments. In the right panel the light solid lines mark the height of dissipation, z_d, for gravity waves with a period 30 min (line A) and 10 hours (line B).

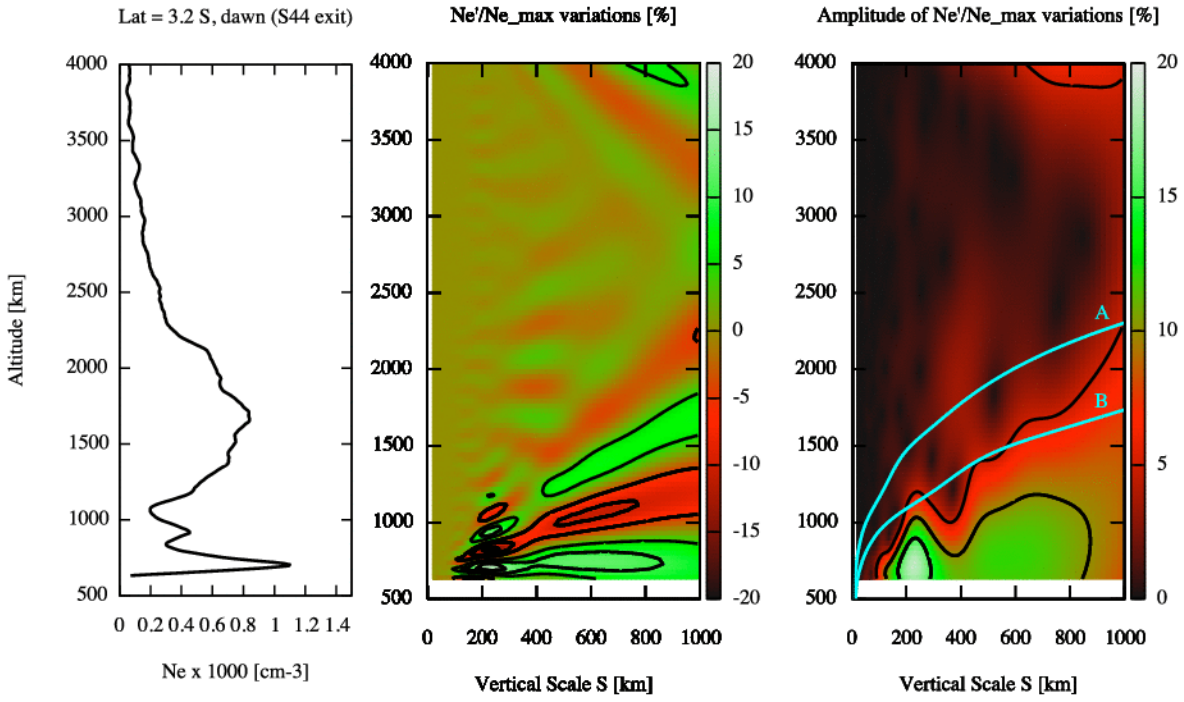

Figure A.13: Low latitude dawn observation (3.2°S). Left panel: Electron density profile from S44 exit radio occultation. Central panel: Electron density variations as a function of scale and altitude. Right panel: Amplitude of the variations as a function of scale and altitude. Contours (solid black lines) are drawn at 5% increments. In the right panel the light solid lines mark the height of dissipation, z_d, for gravity waves with a period 30 min (line A) and 10 hours (line B).

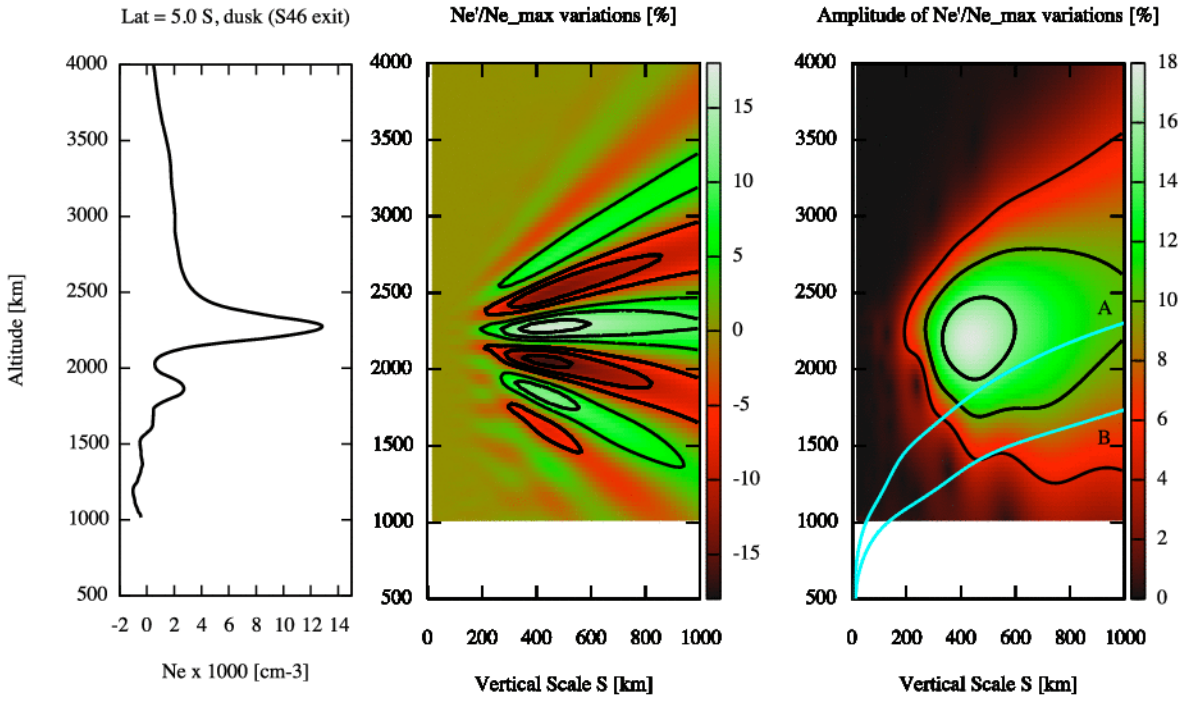

Figure A.14: Low latitude dusk observation (5.0°S). Left panel: Electron density profile from S46 exit radio occultation. Central panel: Electron density variations as a function of scale and altitude. Right panel: Amplitude of the variations as a function of scale and altitude. Contours (solid black lines) are drawn at 5% increments. In the right panel the light solid lines mark the height of dissipation, z_d, for gravity waves with a period 30 min (line A) and 10 hours (line B).

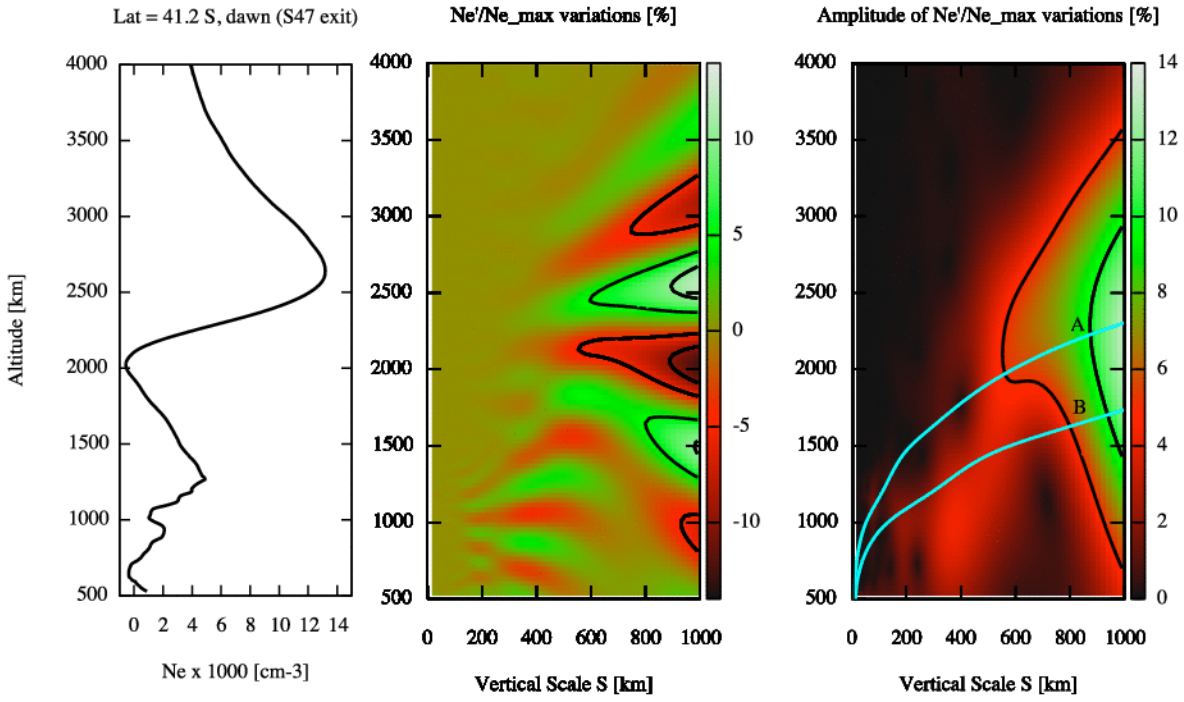

Figure A.15: Middle latitude dawn observation (41.2°N). Left panel: Electron density profile from S47 exit radio occultation. Central panel: Electron density variations as a function of scale and altitude. Right panel: Amplitude of the variations as a function of scale and altitude. Contours (solid black lines) are drawn at 5% increments. In the right panel the light solid lines mark the height of dissipation, z_d, for gravity waves with a period 30 min (line A) and 10 hours (line B).

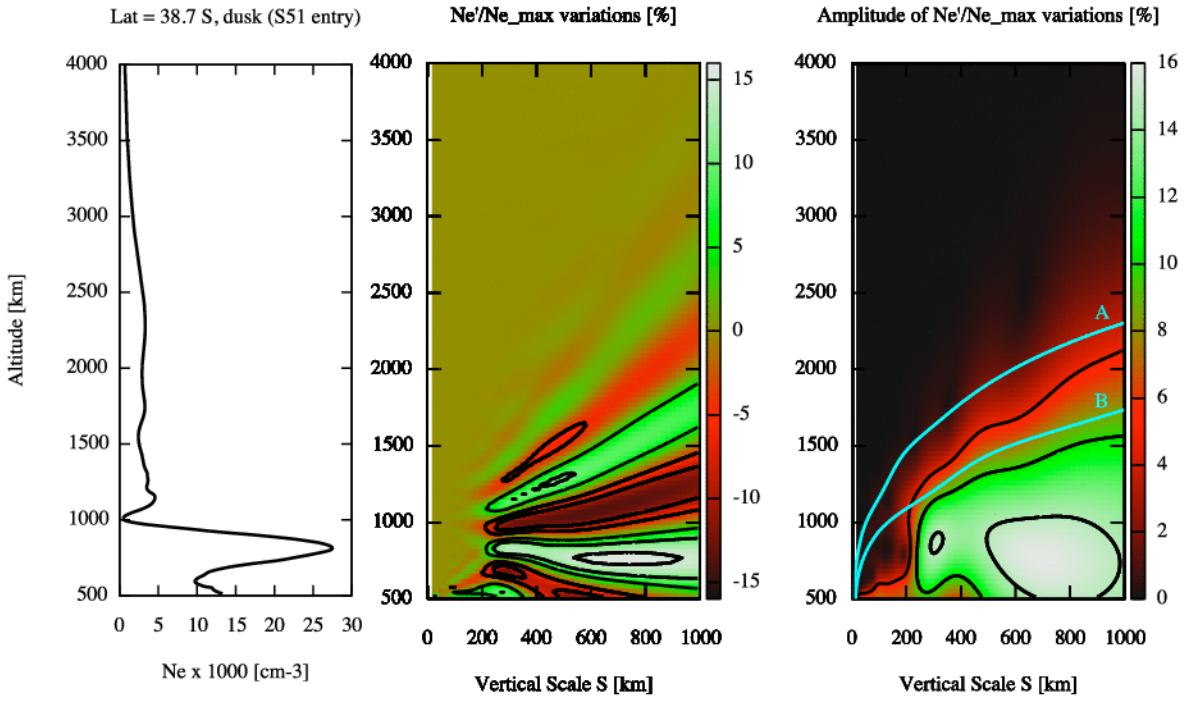

Figure A.16: Middle latitude dusk observation (38.7°S). Left panel: Electron density profile from S51 entry radio occultation. Central panel: Electron density variations as a function of scale and altitude. Right panel: Amplitude of the variations as a function of scale and altitude. Contours (solid black lines) are drawn at 5% increments. In the right panel the light solid lines mark the height of dissipation, z_d, for gravity waves with a period 30 min (line A) and 10 hours (line B).

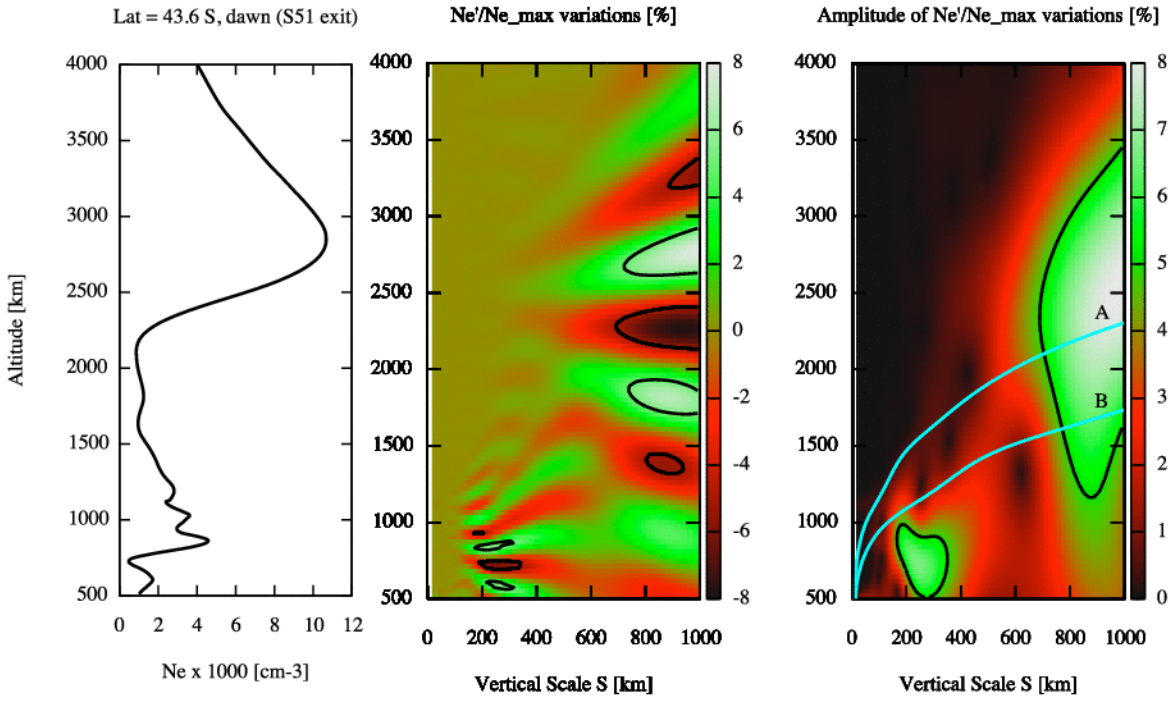

Figure A.17: Middle latitude dawn observation (43.6°S). Left panel: Electron density profile from S51 exit radio occultation. Central panel: Electron density variations as a function of scale and altitude. Right panel: Amplitude of the variations as a function of scale and altitude. Contours (solid black lines) are drawn at 5% increments. In the right panel the light solid lines mark the height of dissipation, z_d, for gravity waves with a period 30 min (line A) and 10 hours (line B).

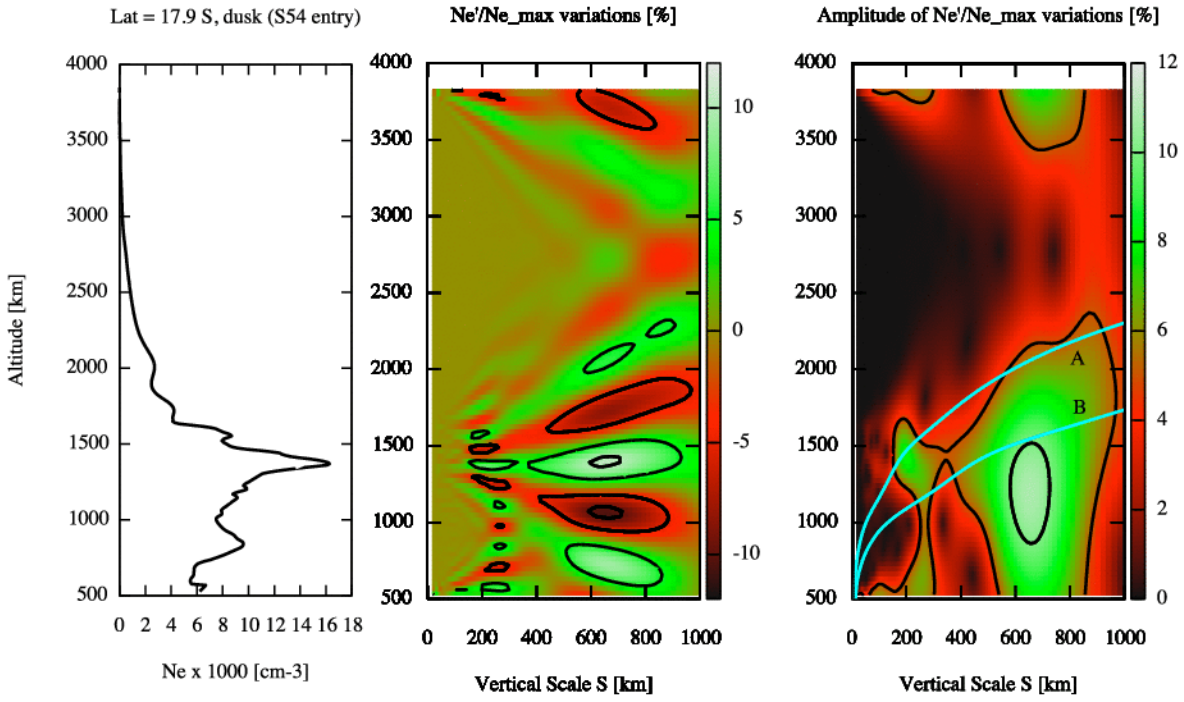

Figure A.18: Low latitude dusk observation (17.9°S). Left panel: Electron density profile from S54 entry radio occultation. Central panel: Electron density variations as a function of scale and altitude. Right panel: Amplitude of the variations as a function of scale and altitude. Contours (solid black lines) are drawn at 5% increments. In the right panel the light solid lines mark the height of dissipation, z_d, for gravity waves with a period 30 min (line A) and 10 hours (line B).

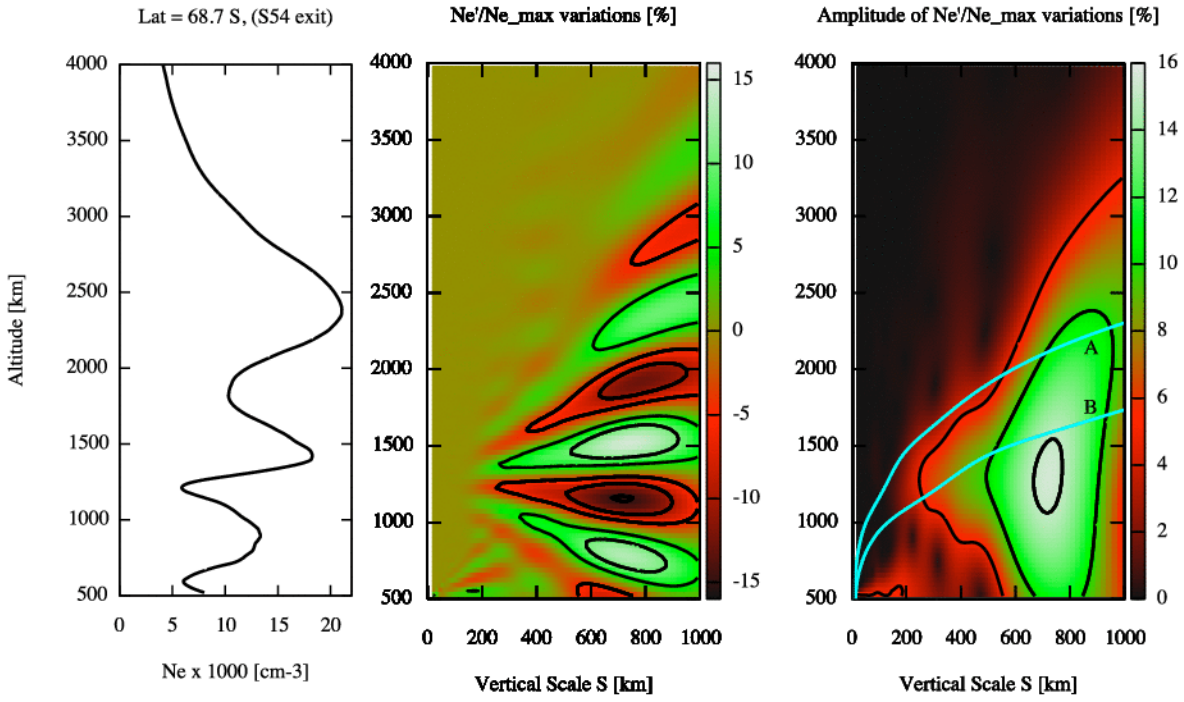

Figure A.19: High latitude observation (68.7°S). Left panel: Electron density profile from S54 exit radio occultation. Central panel: Electron density variations as a function of scale and altitude. Right panel: Amplitude of the variations as a function of scale and altitude. Contours (solid black lines) are drawn at 5% increments. In the right panel the light solid lines mark the height of dissipation, z_d, for gravity waves with a period 30 min (line A) and 10 hours (line B).

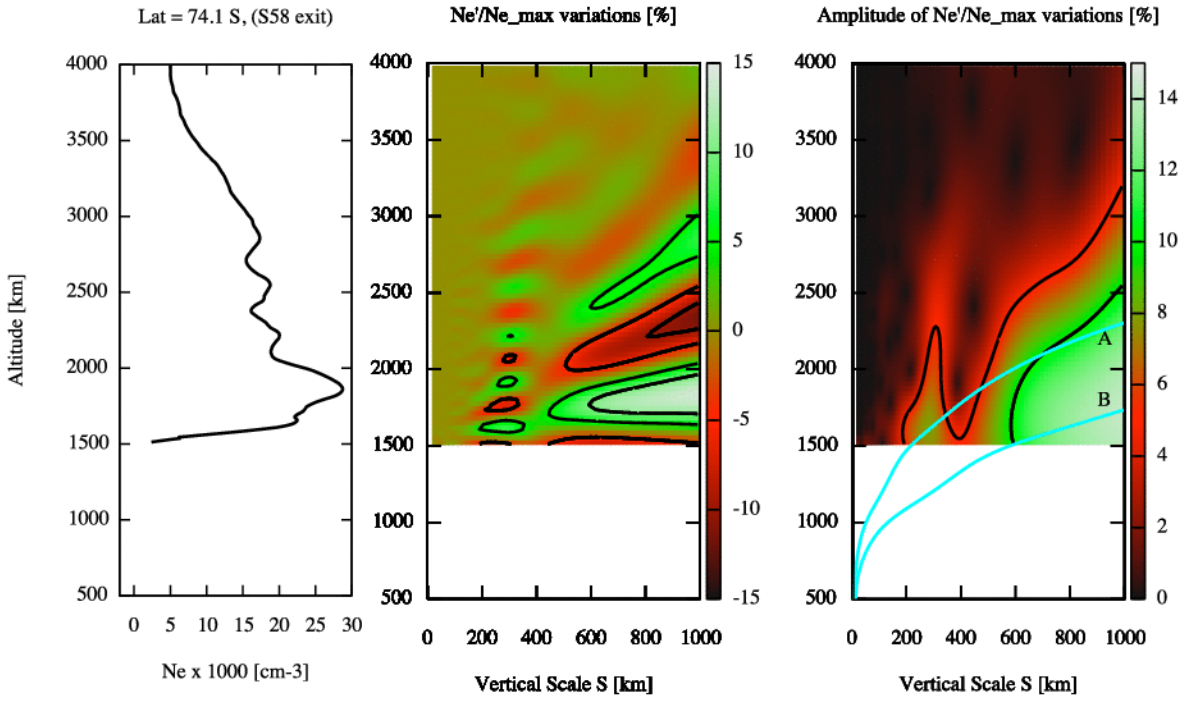

Figure A.20: High latitude observation (74.1°S). Left panel: Electron density profile from S58 exit radio occultation. Central panel: Electron density variations as a function of scale and altitude. Right panel: Amplitude of the variations as a function of scale and altitude. Contours (solid black lines) are drawn at 5% increments. In the right panel the light solid lines mark the height of dissipation, z_d, for gravity waves with a period 30 min (line A) and 10 hours (line B).

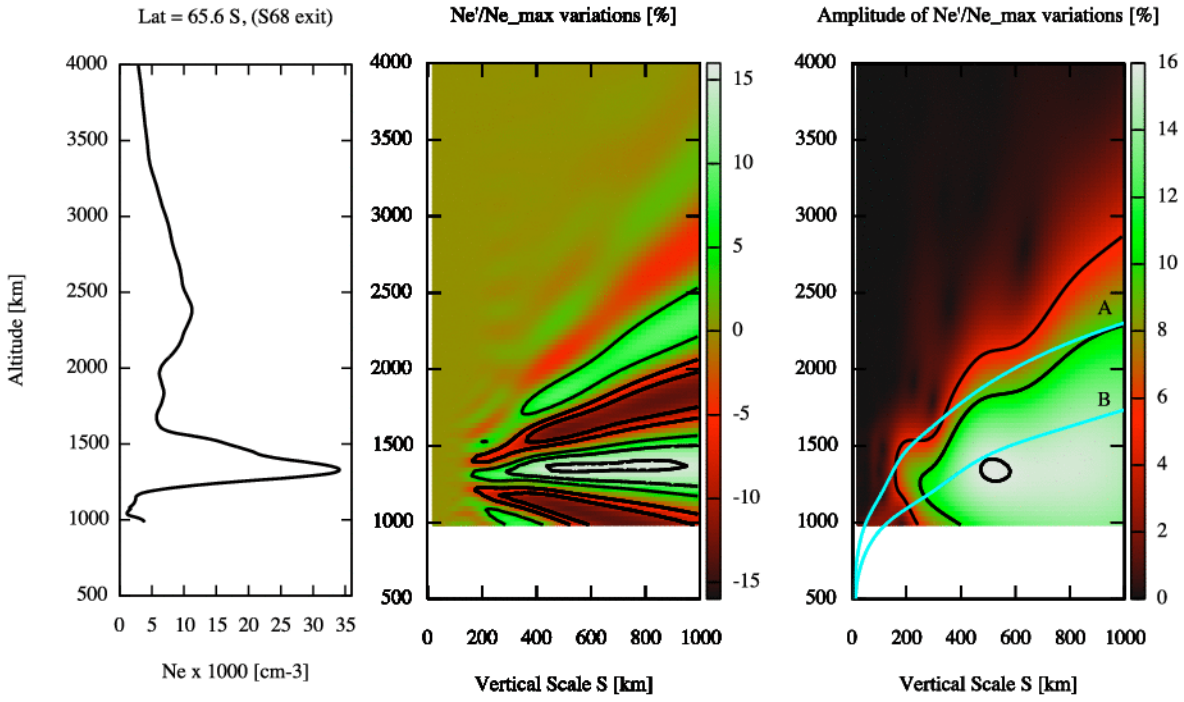

Figure A.21: High latitude observation (65.6°S). Left panel: Electron density profile from S68 exit radio occultation. Central panel: Electron density variations as a function of scale and altitude. Right panel: Amplitude of the variations as a function of scale and altitude. Contours (solid black lines) are drawn at 5% increments. In the right panel the light solid lines mark the height of dissipation, z_d, for gravity waves with a period 30 min (line A) and 10 hours (line B).

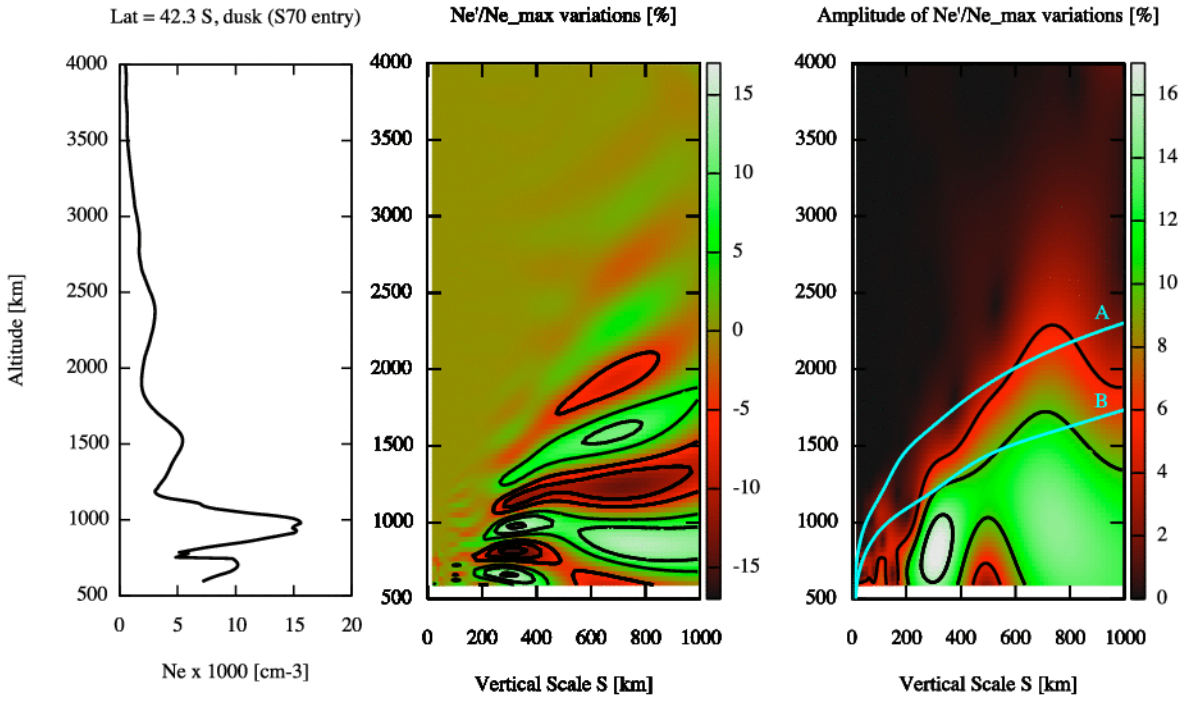

Figure A.22: Middle latitude dusk observation (42.3°S). Left panel: Electron density profile from S70 entry radio occultation. Central panel: Electron density variations as a function of scale and altitude. Right panel: Amplitude of the variations as a function of scale and altitude. Contours (solid black lines) are drawn at 5% increments. In the right panel the light solid lines mark the height of dissipation, z_d, for gravity waves with a period 30 min (line A) and 10 hours (line B).

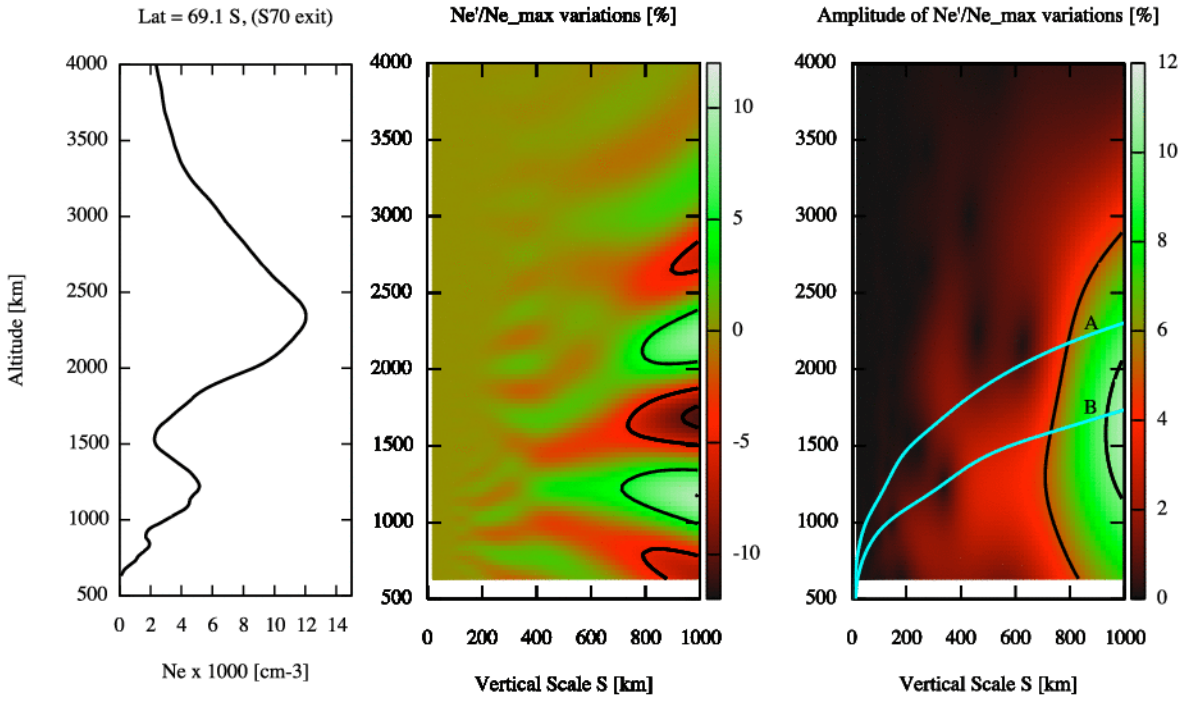

Figure A.23: High latitude observation (69.1°S). Left panel: Electron density profile from S70 exit radio occultation. Central panel: Electron density variations as a function of scale and altitude. Right panel: Amplitude of the variations as a function of scale and altitude. Contours (solid black lines) are drawn at 5% increments. In the right panel the light solid lines mark the height of dissipation, z_d, for gravity waves with a period 30 min (line A) and 10 hours (line B).

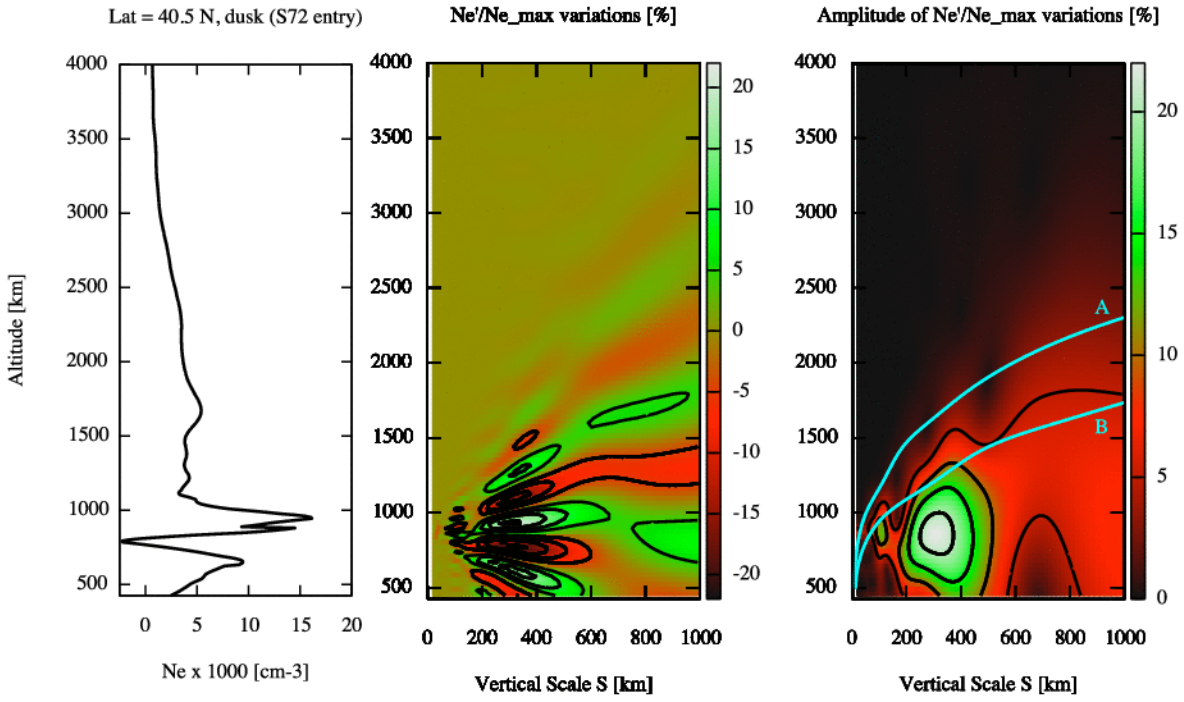

Figure A.24: Middle latitude dusk observation (40.5°N). Left panel: Electron density profile from S72 entry radio occultation. Central panel: Electron density variations as a function of scale and altitude. Right panel: Amplitude of the variations as a function of scale and altitude. Contours (solid black lines) are drawn at 5% increments. In the right panel the light solid lines mark the height of dissipation, z_d, for gravity waves with a period 30 min (line A) and 10 hours (line B).

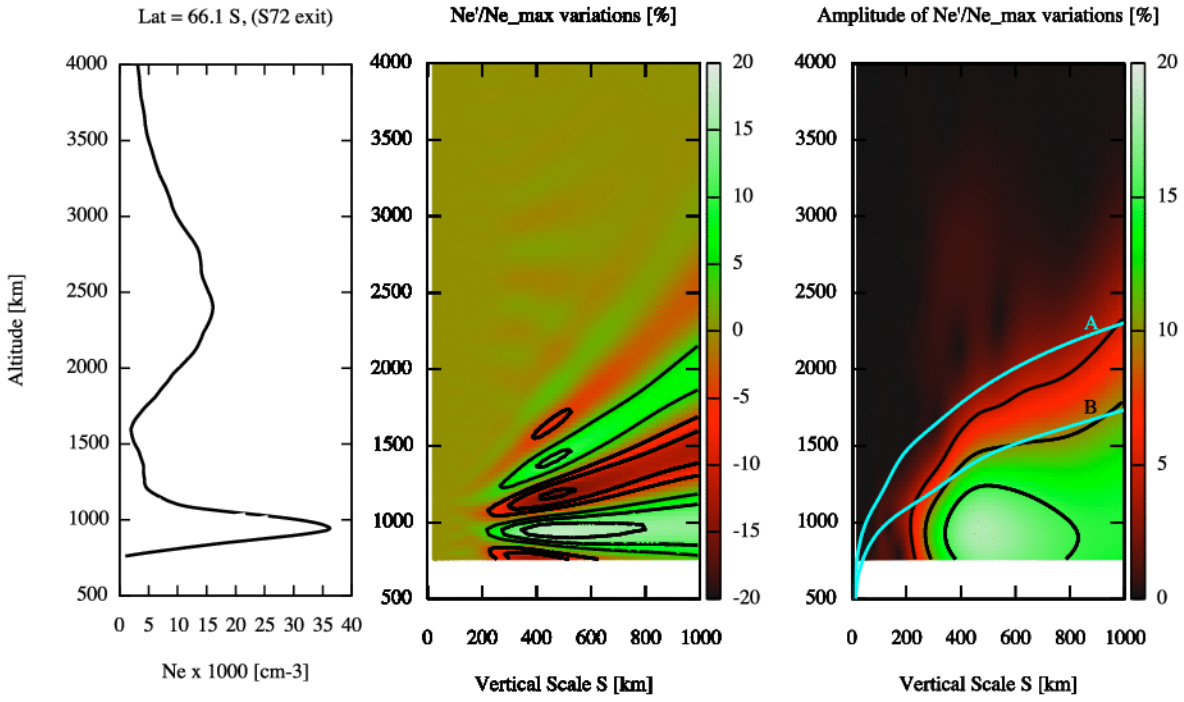

Figure A.25: High latitude observation (66.1°S). Left panel: Electron density profile from S72 exit radio occultation. Central panel: Electron density variations as a function of scale and altitude. Right panel: Amplitude of the variations as a function of scale and altitude. Contours (solid black lines) are drawn at 5% increments. In the right panel the light solid lines mark the height of dissipation, z_d, for gravity waves with a period 30 min (line A) and 10 hours (line B).

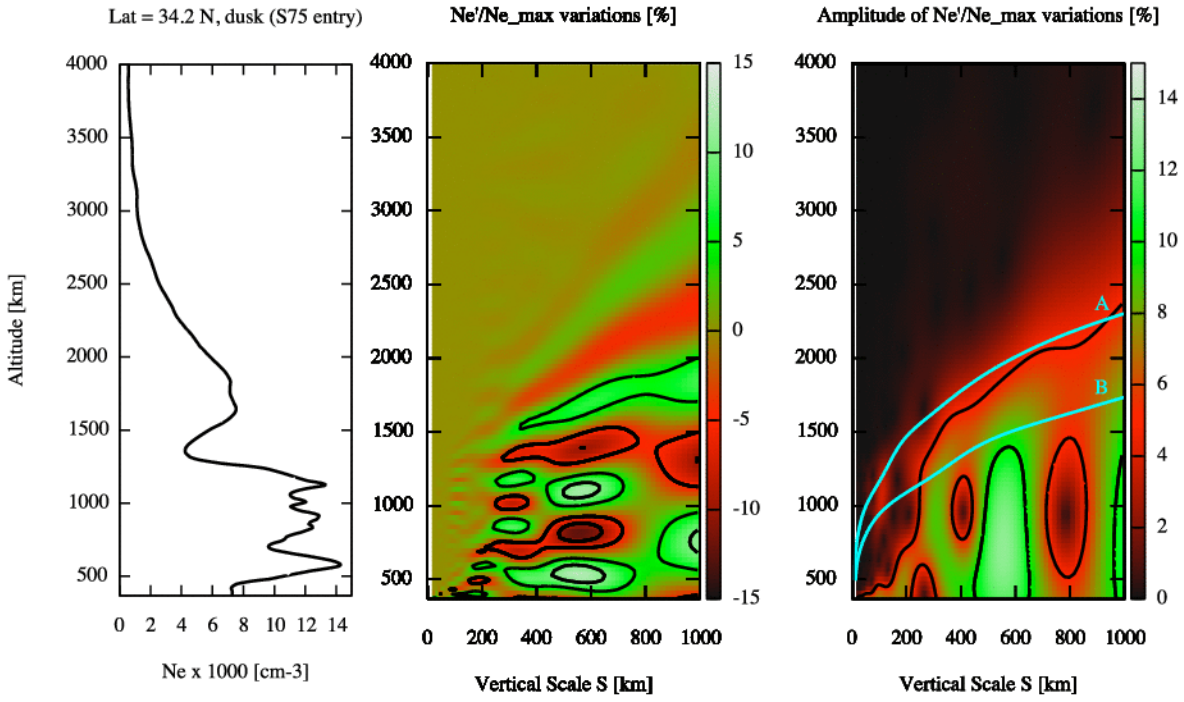

Figure A.26: Middle latitude dusk observation (34.2°N). Left panel: Electron density profile from S75 entry radio occultation. Central panel: Electron density variations as a function of scale and altitude. Right panel: Amplitude of the variations as a function of scale and altitude. Contours (solid black lines) are drawn at 5% increments. In the right panel the light solid lines mark the height of dissipation, z_d, for gravity waves with a period 30 min (line A) and 10 hours (line B).

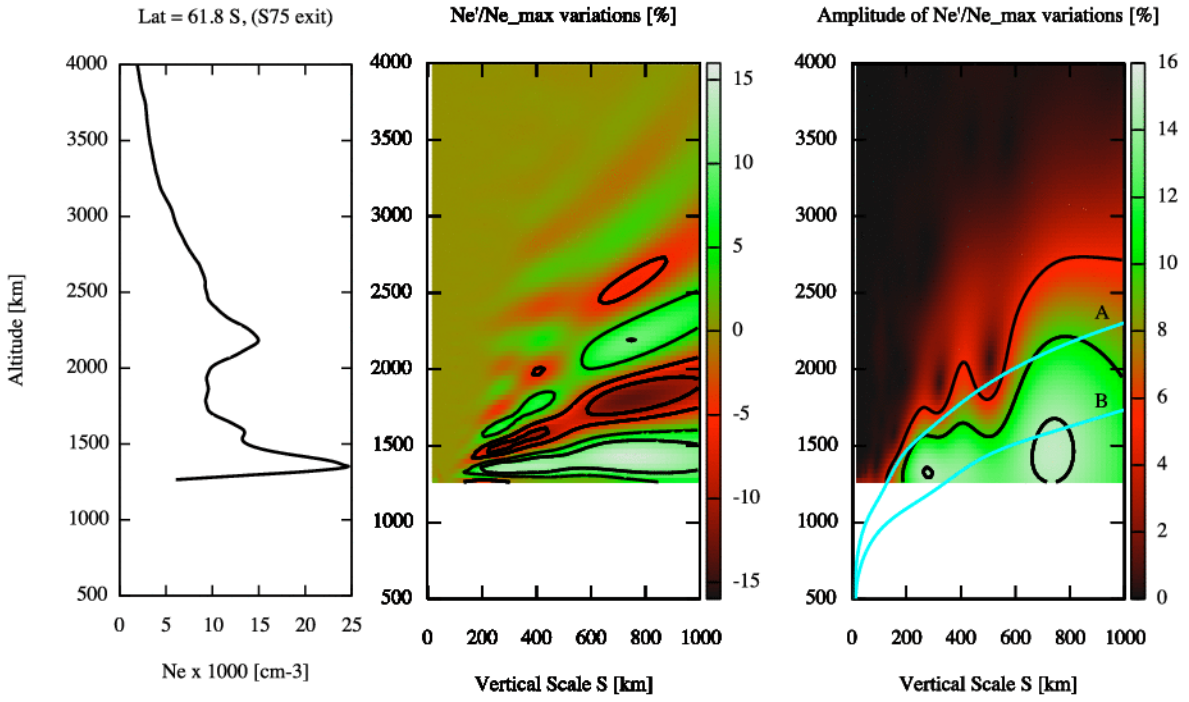

Figure A.27: High latitude observation (61.8°S). Left panel: Electron density profile from S75 exit radio occultation. Central panel: Electron density variations as a function of scale and altitude. Right panel: Amplitude of the variations as a function of scale and altitude. Contours (solid black lines) are drawn at 5% increments. In the right panel the light solid lines mark the height of dissipation, z_d, for gravity waves with a period 30 min (line A) and 10 hours (line B).